FMSN60
Project
Financial Statistics

Modeling volatility, calibration of stock options, and portfolio optimization

Authors

Kajsa Hansson Willis & Victoria Lagerstedt

Lund University

Fall 2025

Contents

1 Intra-day and daily data using standard GARCH-family models and GARCH-x models for volatility **2**
1.1 Data Handling . . . 2
1.1.1 Model Orders . . . 2
1.1.2 Distributions . . . 3
1.2 GARCH . . . 4
1.3 EGARCH . . . 5
1.4 GARCH-X . . . 6
1.5 Testing . . . 8

2 Calibration of Stock Options **10**
2.1 Model Selection . . . 10
2.2 Ordinary Least Squares (OLS) . . . 11
2.3 Penalized Least Squares (PLS) . . . 11
2.3.1 Selection of λ for PLS . . . 11
2.4 The Black & Scholes Model . . . 12
2.5 The Heston Model . . . 13
2.6 The Bates Model . . . 14
2.7 The Carr-Geman-Madan-Yor (CGMY) Model . . . 15
2.8 Analysis . . . 16

3 Portfolio Optimization **19**
3.1 Start-Up . . . 19
3.2 Investment Horizon . . . 19
3.3 Distributions . . . 20
3.4 Estimating Risk Aversion . . . 21
3.5 Statistical Modeling . . . 22
3.5.1 Static Model . . . 22
3.5.2 Rolling window . . . 22
3.5.3 Conditional Mean Modeling . . . 23
3.5.4 Constant Conditional Correlation-GARCH with Gaussian Innovations . . . 25
3.5.5 Constant Conditional Correlation-GARCH with Student-t Innovations . . . 27
3.5.6 Dynamic Conditional Correlation-GARCH for Conditional Covariances with Gaussian Distribution . . . 28
3.6 Choice of Performance Metrics . . . 29
3.6.1 Sharpe Ratio . . . 29
3.6.2 Value-at-Risk . . . 30
3.7 Results . . . 30
3.7.1 Unconditional Covariance . . . 31
3.7.2 Rolling Window . . . 31
3.7.3 CCC-GARCH . . . 32
3.7.4 DCC-GARCH . . . 34
3.7.5 Analysis and Relative Model Validation . . . 35
3.8 Transaction Costs . . . 36

1 Intra-day and daily data using standard GARCH-family models and GARCH-x models for volatility

1.1 Data Handling

1.1.1 Model Orders

In order to create the dynamic volatility models, their order must be determined beforehand. Previous empirical studies have found that GARCH(1,1) models tend to be appropriate and sufficient for capturing volatility dynamics in financial return series and that higher-order extensions typically add little explanatory power (Lindström, Madsen, and Nielsen 2018).

However, the data is examined regardless in order to determine if the (1,1) is appropriate for the specific data set. This is done by analyzing the ACF and the PACF of the squared returns. The squared returns are used as a proxy for the conditional variance in order to investigate the correlation structure of the volatility. These plots can be seen in Figure 1 and 2.

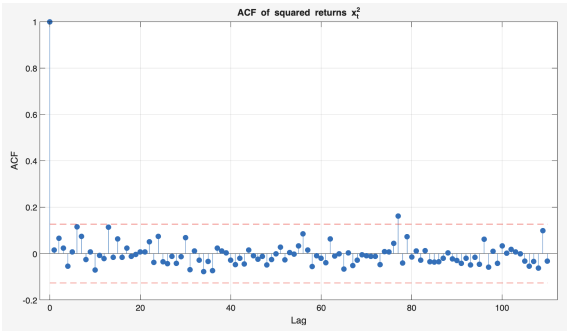

Figure 1: The ACF of the squared return from daily closing prices

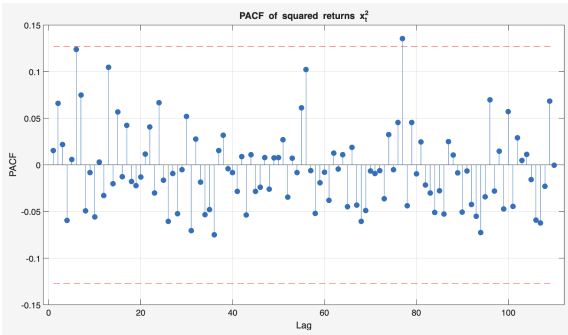

Figure 2: The PACF of the squared return from daily closing prices

The ACF exhibits weak but persistent autocorrelation, while the PACF does not display a clear cutoff or systematic structure beyond the first lag. This suggests limited higher-order dependence in the variance dynamics. Therefore, a GARCH(1,1) specification is deemed sufficient and will be used for all GARCH-type models.

The log-returns were also analyzed and two tests were run to see if the data was stationary. Initially, the ADF test was performed on the data, where the null hypothesis is that the data has a null root. This test gave the result that the null hypothesis could be rejected, meaning the mean is stationary. Then, the KPSS test was run, where stationary data is the null hypothesis. The null hypothesis was failed to be rejected meaning the data is most likely stationary. The conclusion of these tests is that the data can be treated as stationary.

1.1.2 Distributions

Figure 3 shows the daily log returns computed from Volvo closing prices. The series fluctuates around a constant mean with no visible trend or structural breaks, suggesting that the return process is reasonably stationary, agreeing with previously performed tests. This supports the standard modeling assumption of a constant unconditional mean in the volatility models considered.

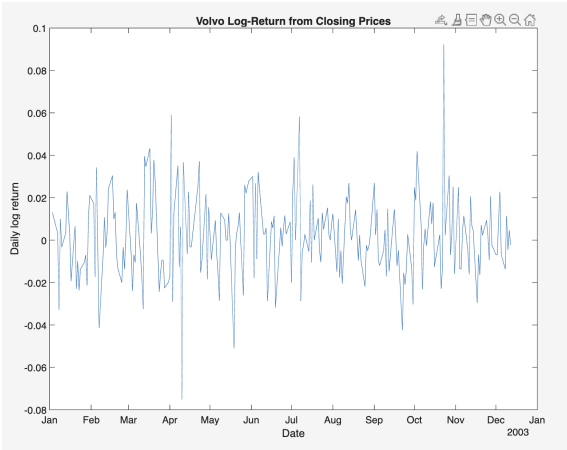

Figure 3: Log returns from daily closing prices of Volvo stock

To assess the distributional properties of the returns, a histogram together with a fitted normal density is shown in Figure 4. The empirical distribution is approximately symmetric and centered around zero, but exhibits slightly heavier tails and center than the Gaussian benchmark. This suggests that while the normal distribution may provide a reasonable first approximation, it may underestimate the probability of extreme or expected observations.

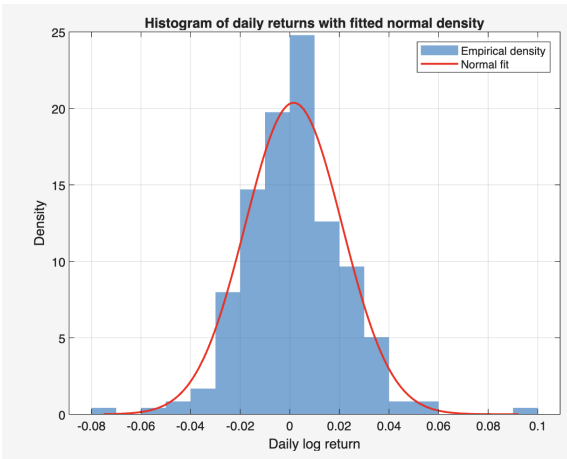

Figure 4: Histogram of daily log returns with fitted normal distribution for Volvo stock

Further insight is provided by the Q-Q plot in Figure 5, which compares the empirical quantiles of the returns to those of a standard normal distribution. While the central part of the distribution aligns well with the 45-degree line, there are some deviations appear in the tails.

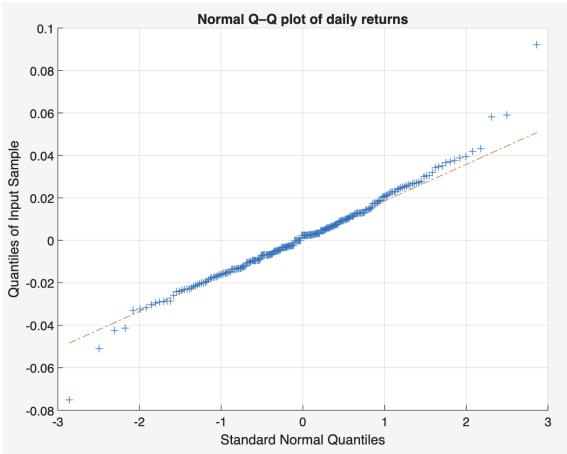

Figure 5: Normal Q-Q plot of daily log returns from closing prices of Volvo stock

Overall, these results suggest that the normal distribution captures the bulk behavior of daily returns reasonably well, especially around the center of the distribution. However, the heavier tails observed in the histogram and Q-Q plot indicate some departure from normality. Nonetheless, the normal distribution appears to be a decent approximation.

1.2 GARCH

A standard GARCH(1,1) model was fitted to the daily log returns from closing prices in order to capture time-varying volatility and volatility clustering according to the lecture notes (Wiktorsson 2025b). The model assumes a constant conditional mean and conditionally Gaussian shocks:

$$r_t = \mu + \varepsilon_t, \qquad \varepsilon_t = \sigma_t z_t, \qquad z_t \sim \mathcal{N}(0,1),$$

with conditional variance evolving according to

$$h_t = \sigma_t^2 = \omega + \alpha\, \varepsilon_{t-1}^2 + \beta\, h_{t-1}.$$

The parameters were estimated by maximum likelihood under the conditional normality assumption. To ensure a well-defined and non-negative volatility process, the constraints below were imposed:

$$\omega > 0, \qquad \alpha \geq 0, \qquad \beta \geq 0, \qquad \alpha + \beta < 1.$$

Under $\alpha + \beta < 1$, the model has finite unconditional variance and the recursion can be initialized using $\mathbb{E}[h_t] = \frac{\omega}{1-\alpha-\beta}$.

Figure 6 shows the estimated conditional volatility $\hat{\sigma}_t = \sqrt{\hat{h}_t}$ over the sample.

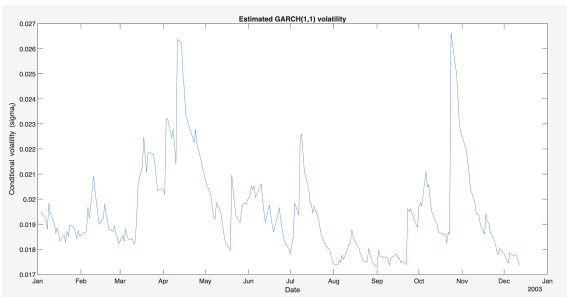

Figure 6: Estimated conditional volatility from the GARCH(1,1) model on daily returns from closing prices of Volvo stock

To connect volatility modeling to return prediction, one-step-ahead forecasts were constructed. Given information at time t, the conditional mean forecast is $\hat{\mu}$ and the one-step-ahead variance forecast is $\widehat{h}_{t+1|t} = \hat{\omega} + \hat{\alpha}\,\hat{\varepsilon}_t^2 + \hat{\beta}\,\hat{h}_t$.

Assuming conditional normality, a 95% prediction interval for r_{t+1} is then $\hat{\mu} \pm z_{0.975}\sqrt{\widehat{h}_{t+1|t}}$.

Figure 7 plots the realized returns together with the forecast band. The width of the interval changes over time in line with the estimated volatility, widening during high-volatility periods and tightening when volatility is low.

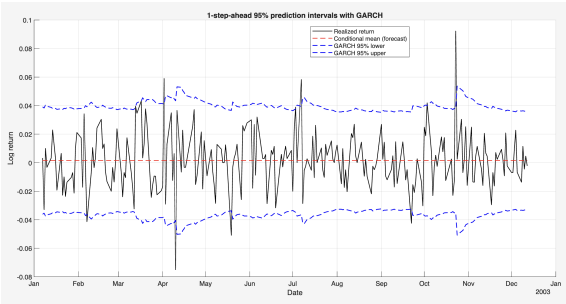

Figure 7: One-step-ahead 95% prediction intervals for log return under the GARCH(1,1) model

The estimated parameters of the GARCH(1,1) model provide further insight into the volatility dynamics of the return series. The conditional mean is estimated as $\hat{\mu} = 0.0014$, indicating a small but positive average daily return. The variance intercept is estimated as $\hat{\omega} = 3.96 \times 10^{-5}$, which is small relative to the overall level of volatility. This suggests that conditional variance is largely driven by past shocks and past volatility rather than by a constant baseline component.

The ARCH coefficient $\hat{\alpha} = 0.0456$ measures the immediate impact of new information on volatility, while the GARCH coefficient $\hat{\beta} = 0.8503$ captures the persistence of volatility over time. Their sum, $\hat{\alpha} + \hat{\beta} = 0.8959$, is close to unity but remains below one, implying a highly persistent yet stationary volatility process.

1.3 EGARCH

To allow for asymmetric volatility responses and to avoid non-negativity constraints on the variance, an EGARCH(1,1) model was also fitted to the daily log returns. The model follows the specification introduced in the course lectures (Wiktorsson 2025b) and is given by:

$$r_t = \mu + \varepsilon_t, \quad \varepsilon_t = w_t\sigma_t, \quad w_t \sim \mathcal{N}(0,1),$$

$$\sigma_t = \exp\left(\tfrac{1}{2}h_t\right),$$

$$h_t = \omega + \alpha w_{t-1} + \beta h_{t-1}$$

In contrast to the standard GARCH model, the EGARCH models the logarithm of the conditional variance. This ensures positivity of σ_t^2 by construction and allows the parameters to take on negative values as well.

The estimated conditional volatility series is shown in Figure 8. Similar to the GARCH model, the EGARCH specification captures pronounced volatility clustering, with periods of elevated volatility followed by gradual mean reversion. The log-linear structure leads to smoother volatility dynamics while still accommodating sharp responses to large shocks.

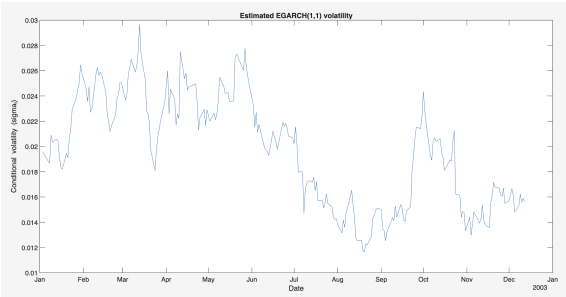

Figure 8: Estimated conditional volatility from the EGARCH(1,1) model on daily returns from closing prices of Volvo stock

One-step-ahead forecasts were constructed in the same way as the GARCH case. Given information at time t, the forecast of the conditional mean is $\hat{\mu}$ and the one-step-ahead forecast of the log-variance is

$$\widehat{h}_{t+1|t} = \hat{\omega} + \hat{\alpha}\,\hat{w}_t + \hat{\beta}\,\hat{h}_t,$$

with $\widehat{\sigma}^2_{t+1|t} = \exp(\widehat{h}_{t+1|t})$. Assuming conditional normality, a 95% prediction interval for r_{t+1} is given by $\hat{\mu} \pm z_{0.975}\,\widehat{\sigma}_{t+1|t}$.

Figure 9 displays the realized returns together with the corresponding EGARCH-based prediction bands. As in the GARCH case, the width of the interval adapts over time in response to changing volatility conditions.

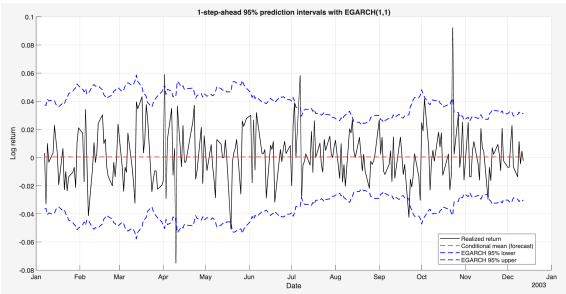

Figure 9: One-step-ahead 95% prediction intervals for log return under the EGARCH(1,1) model.

The estimated parameters provide insight into the volatility dynamics. The conditional mean is estimated as $\hat{\mu} = 0.0005$, indicating a small average daily return. The persistence parameter is estimated as $\hat{\beta} = 0.9990$, suggesting very persistent volatility dynamics.

The asymmetry parameter is estimated as $\hat{\alpha} = -0.1250$. The negative sign indicates that negative shocks tend to increase volatility more than positive shocks of the same magnitude, consistent with a leverage-type effect commonly observed in equity returns. The intercept $\hat{\omega} = -0.0064$ adjusts the long-run level of log-volatility.

Overall, the EGARCH(1,1) model provides a flexible extension of the standard GARCH specification by allowing asymmetric volatility responses and avoiding non-negativity constraints, while delivering volatility and return forecasts comparable in structure to those obtained under the GARCH model.

1.4 GARCH-X

One way to include the intraday data into the variance prediction is to use a GARCH-X model. A GARCH-X model is a version of GARCH models that includes an external variable. The GARCH-X(1,1) volatility function is as follows:

$$\sigma_t^2 = \omega + \alpha\epsilon_{t-1}^2 + \beta\sigma_{t-1}^2 + \gamma x_{t-1}$$

where x is an external variable and $\epsilon_t = X_t - \mu$ (Wiktorsson 2025c).

To use the intraday data as the external variable it needs to be aggregated to the same time scale as the other variables. Therefore, instead of using raw intraday data directly, the intraday data is used to calculate measures such as bi-power variation or quadratic variation, which are then used as the external variables.

The bi-power variation is calculated using Equation 1 (Lindström, Madsen, and Nielsen 2018, page 267) and the quadratic variation for discrete data is calculated using Equation 2 (Haugh 2016).

$$BPV = \frac{\pi}{2} \sum_{n=1}^{N} |X(\tau_{n+1}) - X(\tau_n)||X(\tau_n) - X(\tau_{n-1})| \tag{1}$$

$$QV = \sum_{n=1}^{N} (X(\tau_n) - X(\tau_{n-1}))^2 \tag{2}$$

The Bi-power variation and Quadratic variation each day can be seen in Figure 10. These figures show a clear pattern of the intraday variation being much higher in the beginning of the period than the end.

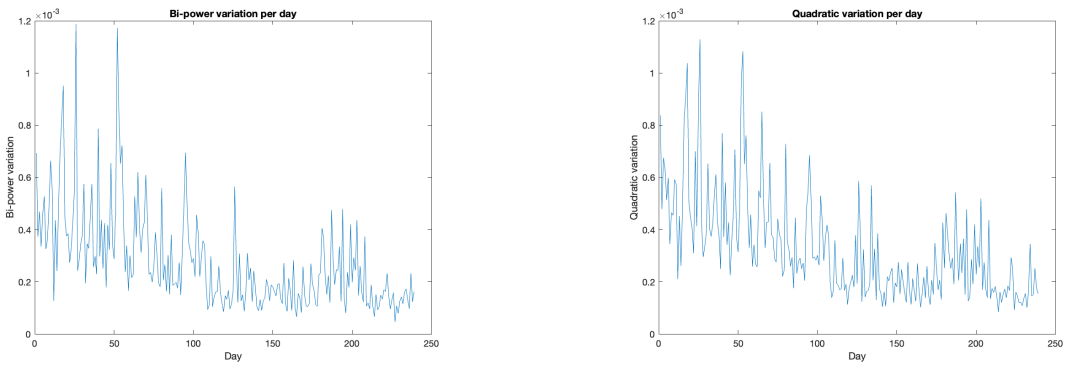

(a) Bi-power variation per day

(b) Quadratic variation per day

Figure 10: Daily bi-power variation and quadratic variation of Volvo stock

To guarantee a well-defined and non-negative volatility process, the constraints below were imposed:

$$\omega > 0, \qquad \alpha \geq 0, \qquad \beta \geq 0.$$

The parameter values in the GARCH-X model were estimated using maximum likelihood and assuming Gaussian distribution. The resulting parameter values can be found in Table 1. The estimated value of ω is zero which suggests the volatility does not have a baseline component and is only driven by the other variables. The estimated alpha value being zero means the past shocks do not affect the volatility at all, making this as persistent process. There are no shocks extreme enough in the data to affect the volatility. The estimated value of the γ-parameter indicates that the external input has some effect on the volatility and the high value of β suggests that the previous volatility has a high impact on future volatilities.

Table 1: Estimated GARCH-X parameters

Parameter	**Estimate using BPV**	**Estimate using QV**
ω	0.0000	0.0000
α	-0.0000	0.0000
β	0.8656	0.8518
γ	0.1467	0.1411
μ	0.0014	0.0015

The resulting volatility per day using this model can be seen in Figure 11. Similar to the bi-power variation and Quadratic variation, the daily volatility is decreasing and is lower in the later half of the year than the first half.

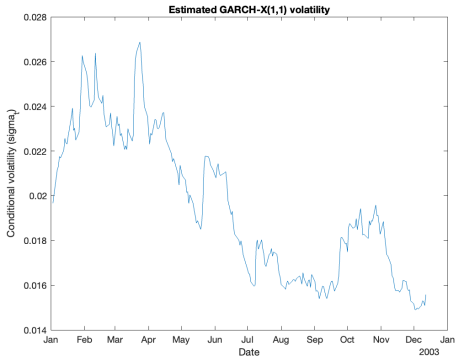

(a) Estimated volatility per day using GARCH-X model with bi-power variation as input

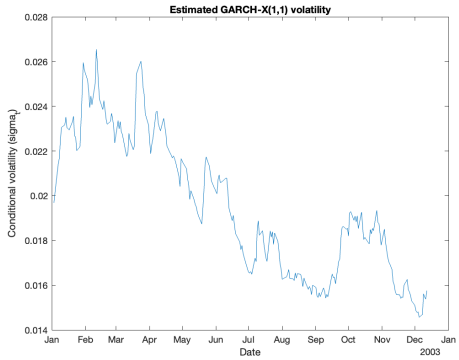

(b) Estimated volatility per day using GARCH-X model with quadratic variation as input

Figure 11: Estimated daily volatility using GARCH-X model on Volvo stock

Using the GARCH-X predicted volatility, a confidence interval of the log returns can be constructed and compared against the real log returns. Figure 12 illustrates the predicted confidence interval for the log returns using the estimated GARCH-X. It is clear the confidence interval captures most of the volatility in the log returns, with only a few large shocks being outside the confidence interval. Therefore, the conclusion is that the GARCH-X model the volatility fairly well.

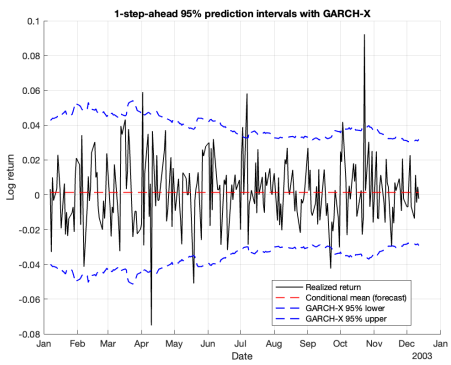

(a) One-step-ahead 95% prediction intervals using bi-power variation as input

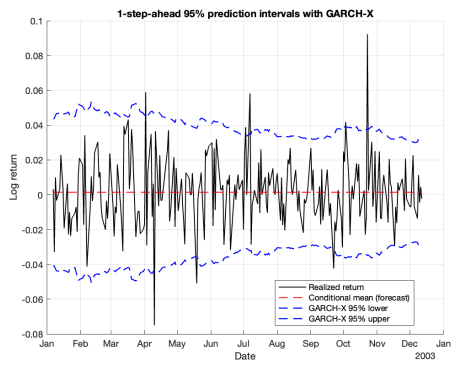

(b) One-step-ahead 95% prediction intervals using quadratic variation as input

Figure 12: One-step-ahead 95% prediction intervals for log return under the GARCH-X(1,1) model

1.5 Testing

The interval predictions were also tested using three testing techniques introduced by Peter F. Christoffersen (Christoffersen 1998). Initially, an indicator variable I_t was defined as the following, where $L_{t|t-1}(p)$ and $U_{t|t-1}(p)$ are the lower and upper bounds of the interval forecast at time t, made at time t-1, and p is the nominal coverage probability.

$$I_t = \begin{cases} 1, & \text{if} \quad y_t \in [L_{t|t-1}(p), U_{t|t-1}(p)] \\ 0, & \text{if} \quad y_t \notin [L_{t|t-1}(p), U_{t|t-1}(p)] \end{cases}$$

The first test was testing conditional coverage using the following likelihood ratio test, where Π_1 is the transition probability matrix of a binary first-order Markov chain.

$$LR_{cc} = -2\ \log[L(p; I_1, I_2, ..., I_T)/L(\hat{\Pi}_1; I_1, I_2, ..., I_T)] \sim^{asy} \chi^2(s(s-1)) = \chi^2(1)$$

Testing for unconditional coverage was performed, using the following likelihood ratio test, where $\hat{\pi} = \frac{n_1}{n_0+n_1}$, n_1 is the number of non-violations, and n_0 is the number of violations.

$$LR_{uc} = -2\ \log[L(p; I_1, I_2, ..., I_T)/L(\hat{\pi}; I_1, I_2, ..., I_T)] \sim^{asy} \chi^2(s-1) = \chi^2(1)$$

The null hypothesis for this test is that the observations are independent Bernoulli trials with success probability p.

Lastly, the likelihood ratio test of independence was performed. The likelihood ratio for this test is the following, where Π_1 is the transition probability matrix of a binary first-order Markov chain and $\hat{\Pi}_2 = (n_{01} + n_{11})/(n_{00} + n_{10} + n_{01} + n_{11})$.

$$LR_{ind} = -2\ \log[L(\hat{\Pi}_2; I_1, I_2, ..., I_T)/L(\hat{\Pi}_1; I_1, I_2, ..., I_T)] \sim^{asy} \chi^2((s-1)^2) = \chi^2(1)$$

The results of these tests on the different models can be seen in Table 2. The null hypothesis failed to be rejected for all the tests on the GARCH and GARCH-X models, meaning that they forecast the Value at Risk well and satisfy conditional coverage, independence, and unconditional coverage at a 5% significance level. The independence test for the EGARCH model rejected the null hypothesis, indicating that violations are clustered under the EGARCH model specifications.

Table 2: Christoffersen Conditional Coverage Tests (5% VaR) of the variance models

Model	**Test**	**LR Statistic**	**Critical Value**	**Result**
GARCH-X with BPV	LR_CC	2.1096	5.9915	Fail to reject H0
	LR_UC	1.4793	3.8415	Fail to reject H0
	LR_IND	0.6303	3.8415	Fail to reject H0
GARCH-X with QV	LR_CC	1.5755	5.9915	Fail to reject H0
	LR_UC	0.7841	3.8415	Fail to reject H0
	LR_IND	0.7914	3.8415	Fail to reject H0
GARCH	LR_CC	1.2920	5.9915	Fail to reject H0
	LR_UC	0.3203	3.8415	Fail to reject H0
	LR_IND	0.9717	3.8415	Fail to reject H0
EGARCH	LR_CC	2.8448	5.9915	Fail to reject H0
	LR_UC	-12.0752	3.8415	Fail to reject H0
	LR_IND	14.9200	3.8415	**Reject H0**

Counting the number of violations using the GARCH-X versus the GARCH model, the GARCH-X have 229 with bi-power variation, 228 with quadratic variation, and GARCH have 227. Therefore, the conclusion is that the external variable does not improve the forecasting performance of the model.

2 Calibration of Stock Options

2.1 Model Selection

In order to calibrate the option prices a model must be selected. While code for option pricing of the Black-Scholes, Heston, Merton, Bates, NIG, NIG-CIR, VG and CGMY models were provided, it was deemed both computationally inefficient and analytically redundant to calibrate every provided model. Instead, a select few were identified as particularly relevant. These were the Black-Scholes model, the Heston model, the Bates model and the Carr-Geman-Madan-Yor (CGMY) model.

The Black-Scholes model is included as a natural benchmark due to its simplicity and its long-standing role in both academic research and practical option pricing. Black-Scholes assumes constant volatility and log-normal asset price dynamics, preventing it from capturing features such as volatility smiles and clustering, and excess kurtosis commonly observed in market data. (Lindström, Madsen, and Nielsen 2018)

The Heston model extends the Black-Scholes model by introducing stochastic volatility through a mean-reverting square-root process. This allows the model to capture volatility smiles and skews commonly observed in options. In addition, the correlation between the asset price and volatility innovations introduces leverage effects frequently seen in markets. The Heston model is therefore an appropriate next step in model complexity. (Heston 1993)

While the Heston model captures stochastic volatility, it still assumes continuous price paths. The Bates model further extends Heston by incorporating jumps in the underlying asset price via a compound Poisson process. This allows the model to better account for short-term maturity options and sharp movements in option prices that cannot be explained by stochastic volatility alone. The Bates model therefore provides a framework that combines both stochastic volatility and jump risk, making it an appropriate next step in the stock option calibration. (Zaevski, Kim, and Fabozzi 2014)

The CGMY model extends the class of exponential Lévy models by allowing for infinite-activity jump processes with flexible tail behavior. The model is characterized by four parameters controlling the intensity, asymmetry, and activity of jumps, enabling it to capture heavy tails and skewness commonly observed in asset returns. Unlike Brownian-driven models, CGMY does not rely on stochastic volatility, but instead reproduces volatility smiles through its jump structure. It is a flexible modeling framework capturing non-Gaussian characteristics of asset returns without introducing excessive model complexity. The CGMY model is therefore included to assess how well jump-driven dynamics alone can explain observed option prices, compared to models that rely on stochastic volatility. (Carr et al. 2002)

While several additional models were available these were not included in the calibration exercise in order to maintain a balance between model diversity and analytical focus. Many of these models share structural similarities with the ones selected and would therefore provide limited additional insight. For example, the Merton model incorporates jumps in asset prices but maintains constant volatility, effectively making it a special case of the Bates model, which allows for both stochastic volatility and jump components. Similarly, the VG and NIG models belong to the same class of pure-jump exponential Lévy models as CGMY. They differ mainly in how the jump intensity, asymmetry, and tail behavior are parameterized, rather than in the underlying modeling framework. Including multiple models from the same structural class would increase computational complexity without substantially improving the comparative analysis. Thus, the selected set of models covers a broad range of dynamics, including constant volatility, stochastic volatility, jump–diffusion, and pure-jump processes, allowing for a meaningful comparison of how different sources of randomness contribute to option pricing.

The NIG–CIR model was also briefly considered, as it combines two important extensions of the Black–Scholes framework. Asset returns are modeled using a Normal Inverse Gaussian (NIG) Lévy process, allowing for asymmetric heavy-tailed return distributions, while the time change is driven by the integrated variance of a Cox–Ingersoll–Ross (CIR) process. This construction introduces stochastic volatility in an indirect but flexible way, enabling the model to jointly capture jump-driven return behavior and volatility clustering. (Belomestny 2011)

Despite these appealing features, the NIG–CIR model introduces a substantial increase in model complexity relative to the insight it would be expected to provide. In particular, it combines

characteristics already explored separately by the Bates and CGMY models making it less suitable as a distinct point of comparison. In addition, the calibration of time-changed Lévy models is computationally demanding and often suffers from weak parameter identification in finite samples. For these reasons, the NIG–CIR model was excluded from the calibration.

2.2 Ordinary Least Squares (OLS)

First, the parameters will be estimated using Ordinary Least Squares. Under OLS, parameters are estimated independently at each time index by minimizing the sum of squared pricing errors across the available option cross-section:

$$\min_{\theta_t} \sum_{i=1}^{N_t} \left(C_i^{\text{model}}(\theta_t) - C_{i,t}^{\text{mkt}} \right)^2 ,$$

where N_t denotes the number of traded options at time t. $C_i^{\text{model}}(\theta_t)$ denotes the model-implied option price and $C_{i,t}^{\text{mkt}}$ is the corresponding market mid-quote.

OLS calibration treats each option surface independently and therefore prioritizes local fit to market prices. While this approach can achieve a close fit at each time index, it may result in highly variable parameter estimates over time, especially for models with many parameters such as Heston, Bates, and CGMY. This instability can lead to financially implausible parameter jumps and complicates interpretation of the estimated dynamics.

2.3 Penalized Least Squares (PLS)

To address the temporal instability in the OLS calibration, a Penalized Least Squares approach is also employed. The PLS method expands the OLS objective with a penalty term, λ, that discourages large deviations from the parameter estimates obtained at the previous time index.

For a parameter vector $\theta_t = (v_{0,t}, \kappa_t, \theta_t, \sigma_t, \rho_t)^\top$, the penalized objective function is given by

$$\min_{\theta_t} \sum_{i=1}^{N_t} \left(C_i^{\text{model}}(\theta_t) - C_{i,t}^{\text{mkt}} \right)^2 \; + \; \lambda \, \|\theta_t - \theta_{t-1}\|^2 \tag{3}$$

where $\lambda > 0$ controls the strength of the penalization.

The penalty term enforces temporal smoothness of the estimated parameter paths, reducing excessive variability while still allowing parameters to evolve over time. When $\lambda = 0$, the PLS estimator reduces to standard OLS.

In practice, the optimization problem is solved using MATLAB's `lsqnonlin` routine (MathWorks, Inc. 2025) by stacking the pricing residuals and the penalty term into a single least squares vector, as seen in (4).

$$F(\theta_t) = \begin{pmatrix} C^{\text{model}}(\theta_t) - C_t^{\text{mkt}} \\ \sqrt{\lambda}\,(\theta_t - \theta_{t-1}) \end{pmatrix}, \tag{4}$$

so that the resulting least squares objective corresponds exactly to (3).

The initial parameter vector θ_1 is obtained by ordinary least squares calibration at the first time index.

2.3.1 Selection of λ for PLS

The choice of the penalty parameter λ determines the trade-off between goodness-of-fit and temporal smoothness. Small values of λ yield estimates close to OLS, while larger values increasingly smooth the parameter trajectories.

In this exercise, λ was fixed at $\lambda = 5$ across all PLS calibrations. Preliminary experimentation indicated that smaller values ($\lambda = 1$ for example) resulted in parameter trajectories that were nearly indistinguishable from OLS estimates, while larger values ($\lambda = 10$ for example) provided much stabilization. The chosen value therefore represents a compromise between goodness-of-fit to individual option cross-sections and temporal smoothness of the estimated parameters.

Estimates with the Heston model with different values of λ can be seen in Figures 13 and 14. These served as a basis for selecting $\lambda = 5$ as it seemed like the better compromise. Further testing of which value was most appropriate through for instance RMSE was considered, but it was decided that these empirical tests were adequate for the selection.

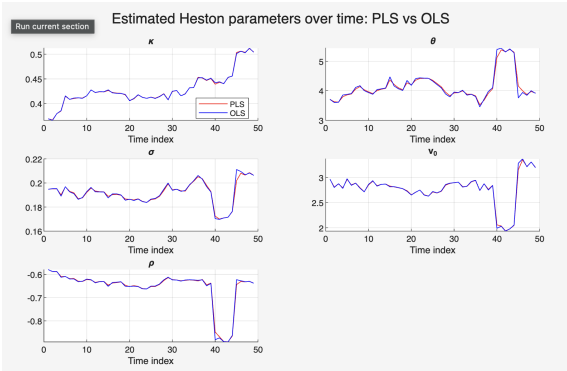

Figure 13: Heston model parameters from OLS and PLS estimation with $\lambda = 5$

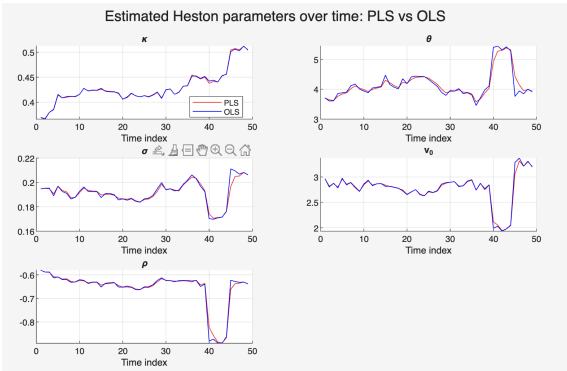

Figure 14: Heston model parameters from OLS and PLS estimation with $\lambda = 10$

Importantly, λ was kept constant across models to ensure comparability of results and to avoid introducing additional model-specific tuning parameters. The focus is thus placed on relative model performance rather than fine-tuning the regularization strength.

2.4 The Black & Scholes Model

The Black-Scholes (BS) model serves as a benchmark for the option calibration exercise. Under the risk-neutral measure, the underlying asset price is assumed to follow a geometric Brownian motion,

$$dS(t) = rS(t)dt + \sigma S(t)dW(t), \sigma > 0$$

where r denotes the constant risk-free rate, σ is the constant volatility parameter, and $W(t)$ is a standard Brownian motion. The model assumes that log-returns are normally distributed and that option prices depend on a single volatility parameter. (Lindström, Madsen, and Nielsen 2018)

Despite its restrictive assumptions, the Black-Scholes model remains a useful reference point. Its analytical simplicity enables efficient calibration and offers a natural reference point for evaluating more complex models. In this way, any improvements in fit obtained from stochastic volatility or jump-based specifications can be assessed relative to the BS benchmark.

Model parameters were calibrated using the estimation methodology previously described. Both the OLS and the PLS were used to obtain a time series of implied volatility estimates. Under

OLS, each option cross-section is fitted independently, while the PLS approach enforces temporal smoothness in the volatility estimates.

Figure 15 displays the implied volatility estimates obtained via OLS. The estimates exhibit some variability over time, reflecting the sensitivity of the OLS procedure to local changes in option prices. Figure 16 shows the corresponding PLS estimates, which are a little smoother due to the penalization term. However, there are only very small differences.

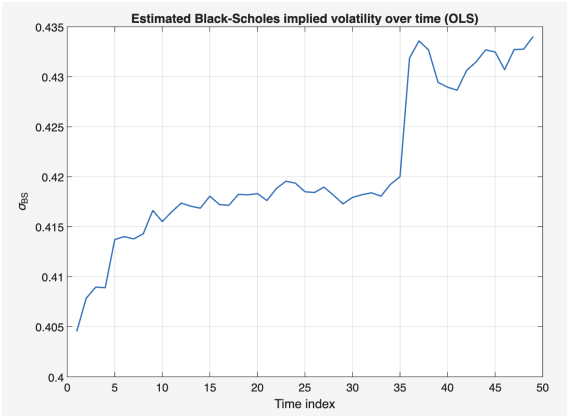

Figure 15: Implied volatility estimate under the Black-Scholes model using ordinary least squares (OLS)

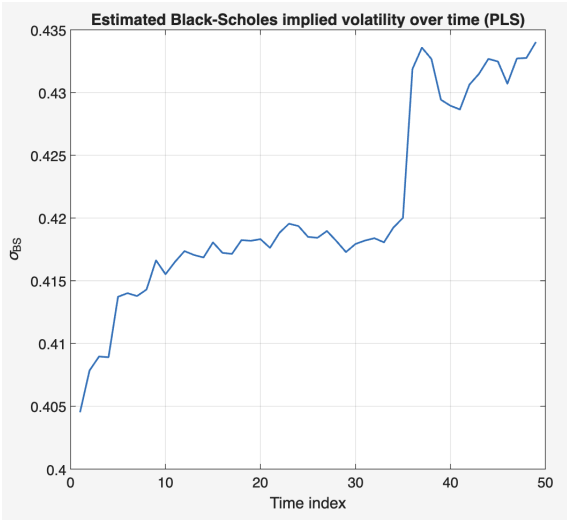

Figure 16: Implied volatility estimate under the Black-Scholes model using penalized least squares (PLS)

2.5 The Heston Model

The Heston model extends the Black-Scholes framework by allowing the volatility of the underlying asset to evolve stochastically over time. This additional flexibility enables the model to capture important empirical features of option prices such as volatility smiles, skews, and leverage effects that cannot be reproduced under constant volatility assumptions.

Under the risk-neutral measure, the Heston model is defined by

$$\begin{aligned} dS_t &= rS_t\,dt + \sqrt{v_t}\,S_t\,dW_t^S, \\ dv_t &= \kappa(\theta - v_t)\,dt + \sigma\sqrt{v_t}\,dW_t^v, \\ dW_t^S\,dW_t^v &= \rho\,dt \end{aligned}$$

where v_t denotes the instantaneous variance process. The parameter κ governs the speed of mean reversion toward the long-run variance level θ, σ controls the volatility of volatility, and ρ captures the correlation between innovations in the asset price and variance processes. To ensure that the variance process remains strictly positive, the Feller condition

$$2\kappa\theta \geq \sigma^2$$

is required. (Heston 1993)

Compared to the BS model, the Heston specification introduces additional parameters and a richer dynamic structure. While this increases model complexity, it allows the model to reproduce empirically observed option pricing patterns that are unattainable under constant volatility.

Calibration of the Heston model was performed using both ordinary least squares (OLS) and penalized least squares (PLS), as described earlier. The OLS approach estimates parameters independently at each time index, prioritizing local fit to option prices. In contrast, the PLS approach introduces a temporal smoothness penalty that stabilizes the parameter paths over time, which is important for multi-parameter models such as Heston.

Figure 17 illustrates the evolution of the estimated Heston parameters under OLS and PLS calibration. The OLS estimates exhibit variability over time, reflecting sensitivity to local option market conditions. The PLS estimates are a bit smoother, indicating that penalization mitigates some estimation noise while still allowing parameters to evolve in response to changing market conditions.

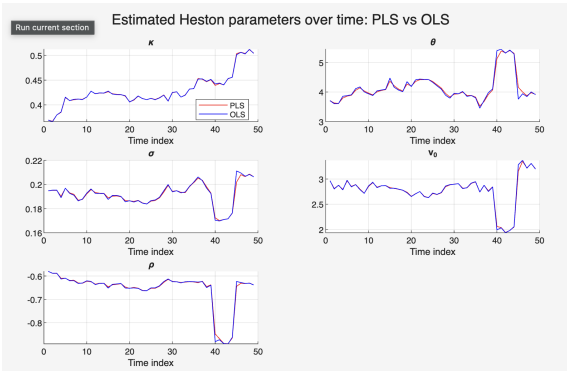

Figure 17: Comparison of OLS and PLS parameter estimates for the Heston model

2.6 The Bates Model

The Bates model further extends the Heston stochastic volatility framework by incorporating discontinuous jumps in the underlying asset price. By allowing for both stochastic volatility and jump risk, the model is able to capture sudden large movements in asset prices and short-maturity option behavior that cannot be explained by continuous-path models alone.

Under the risk-neutral measure, the Bates model dynamics are given by

$$\begin{aligned} dS(t) &= rS(t)\,dt + \sqrt{V(t)}\,S(t)\,dW_1(t) + S(t)\big(e^{J(t)} - 1\big)\,dN(t) - a_j S(t)\,dt, \\ dV(t) &= \kappa(\theta - V(t))\,dt + \sigma\sqrt{V(t)}\,dW_2(t), \\ dW_1(t)\,dW_2(t) &= \rho\,dt \end{aligned}$$

where $V(t)$ denotes the instantaneous variance process. The jump component is driven by a Poisson process $N(t)$ with intensity λ, and jump sizes $J(t)$ are assumed to be normally distributed with mean μ_J and variance σ_J^2. The compensator term

$$a_j = \lambda\left(e^{\mu_J + \frac{1}{2}\sigma_J^2} - 1\right)$$

ensures that the discounted asset price remains a martingale under the risk-neutral measure. (Bates 1996)

Relative to the Heston model, the Bates specification introduces additional parameters governing the frequency and magnitude of jumps. This increased flexibility allows the model to better match option prices with pronounced skewness and kurtosis, particularly for short maturities and deep out-of-the-money options.

Calibration of the Bates model was conducted using both ordinary least squares (OLS) and penalized least squares (PLS), following the methodology described earlier. As with the Heston case, OLS calibration prioritizes local fit to each option cross-section, while PLS imposes temporal smoothness on the parameter paths to reduce estimation instability.

Figure 18 compares the evolution of the estimated Bates parameters under OLS and PLS calibration. The OLS estimates display greater variability over time. In contrast, the PLS estimates are considerably smoother, with the exception of the time index, indicating that the penalization manages to stabilize the estimation of both volatility and jump-related parameters without eliminating meaningful time variation.

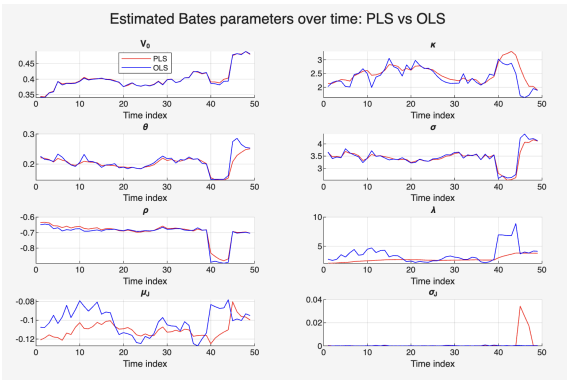

Figure 18: Comparison of OLS and PLS parameter estimates for Bates

2.7 The Carr-Geman-Madan-Yor (CGMY) Model

The Carr-Geman-Madan-Yor (CGMY) model belongs to the class of exponential Lévy models and captures asset price dynamics entirely through a pure-jump process. Unlike the previous models, CGMY does not rely on a Brownian diffusion or stochastic volatility. Instead, it generates implied volatility smiles through its flexible jump structure.

Under the risk-neutral measure, the asset price follows

$$S(t) = S(0) \exp\big(r_t + X(t)\big)$$

where $X(t)$ is a Lévy process characterized by the four CGMY parameters (C, G, M, Y). These parameters control the overall jump intensity (C), the asymmetry between upward and downward jumps (G and M), and the activity level of small jumps (Y). The parameter $Y \in (0, 2)$ determines the degree of jump activity, with larger values corresponding to infinite-activity jump behavior and heavier tails. (Carr et al. 2002)

As the CGMY model can generate volatility smiles without introducing stochastic volatility, it is a useful benchmark for assessing how much of the observed option price structure can be explained by jump dynamics alone.

Calibration of the CGMY model was performed using both ordinary least squares (OLS) and penalized least squares (PLS), following the same methodology applied to the previous models. As CGMY is a pure-jump model with no latent variance process, its parameters are inferred solely from the cross-sectional shape of option prices.

Figure 19 compares the estimated CGMY parameters under OLS and PLS calibration. The OLS estimates exhibit substantial variability over time, reflecting the high flexibility of the model and its sensitivity to noise in individual option surfaces. While the PLS approach reduces some of this variability by enforcing temporal smoothness, the parameter paths remain relatively unstable compared to those obtained for diffusion-based models. The difference is especially salient for the M-parameter, but the parameters vary considerably for all parameters.

This behavior highlights an important trade-off inherent in pure-jump specifications. Although the CGMY model is highly expressive and capable of fitting complex option price patterns, its increased flexibility can lead to weaker parameter identification in finite samples. As a result, even with penalization, CGMY parameters may display considerable time variation, particularly when calibrated across option cross-sections.

Despite these challenges, the CGMY model provides valuable insight into the role of jump-driven dynamics in option pricing and serves as a useful contrast to models that rely on stochastic volatility to explain implied volatility structures.

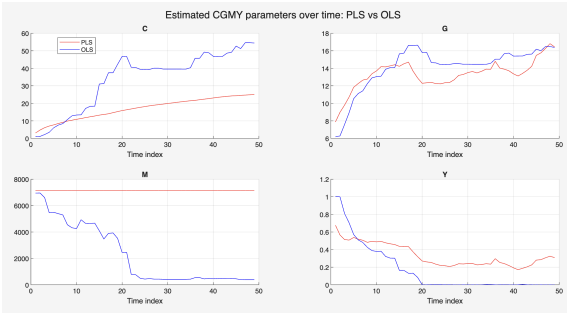

Figure 19: Comparison of OLS and PLS parameter estimates for CGMY

2.8 Analysis

A subset of the data of the first ten time steps was chosen as the training set for the parameter estimates. Further analysis was made using a model with the estimated parameters at time 10 for the different models.

To compare predictive option pricing performance of the different models, mean absolute error, mean squared error and root mean squared error were used. A good base metric to use to test performance of the models is mean absolute error due to it penalizing all errors proportional. The inclusion of mean squared error was made because it strongly penalizes large errors. It is important for a model to not give any really large errors since they can have a severe effect on outcome. Root mean squared error was also used because it is easier to interpret financially than the others.

$$MAE = \frac{1}{n}\sum |y_i - \hat{y}_i| \tag{5}$$

$$MSE = \frac{1}{n}\sum (y_i - \hat{y}_i)^2 \tag{6}$$

$$RMSE = \sqrt{\frac{1}{n}\sum (y_i - \hat{y}_i)^2} \tag{7}$$

Initially, the errors of the different models were analyzed in the time dimension. The option prices at different time points were calculated using the estimated parameters at the end of the training data for the different models. The predicted values were compared against the mid prices by calculating the different error metrics. The result of this analysis can be seen in Figure 20. Observing the graphs it is clear that the errors increase for increasing time points. It is noteworthy that the errors associated with the Heston and Bates models remain relatively stable up to approximately time point 35, after which a pronounced increase is observed. This behavior could be due to a structural change in the underlying data, causing the previously estimated parameter to lose adequacy and reducing the models' ability to accurately capture the dynamics beyond this point. Analysis of the time series of the estimated parameters which was previously done shows a pronounced change in the Heston and Bates models at time point 40, suggesting the possibility of a regime shift in the option price dynamics. The Heston and Bates model does have a state variable and mean reversion. When the market conditions are calm these models provide stable pricing but when there exist volatility jumps the state variable might be misaligned and the model reacts too slowly. This might be the reason for seeing the high peaks in Figure 20. The Black & Scholes

and CGMY models exhibit another behavior, where the errors instead gradually increase as time increases. The Black & Scholes model and CGMY model have no other state variables than the asset price and all randomness is driven by one Brownian motion or Lévy process. Therefore, the model does not adapt dynamically and errors will accumulate gradually. The conclusion from all these models is that the predictive performance deteriorates as the forecast horizon increases.

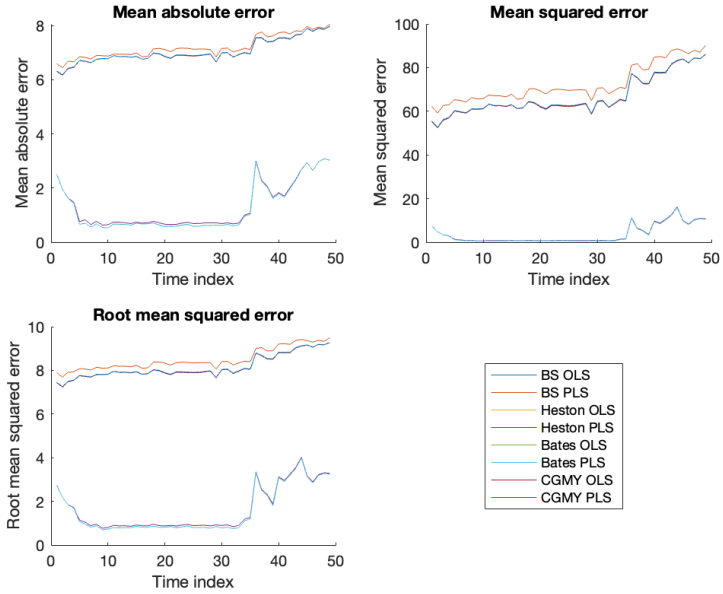

Figure 20: Comparison of different error metrics in the time dimension

It is also interesting to analyze the maturity dimension, how well the models perform for different time to maturities; see Figure 21. The largest errors for the Black & Scholes and CGMY models occur at around time to maturity 0.4-0.7 and at really low time to maturities. The errors for the Heston and Bates models behave different where instead the highest errors occur around time to maturities 0.4-0.7 and the smallest errors at the highest and lowest time to maturities. The U-shaped error profile for the Black & Scholes and CGMY models might be due to them having no stochastic volatility, which gives them an inability to match short-term volatility skew and long-term variance dynamics. The inverted U-shape for the Heston and Bates models has its largest errors in the middle of the maturity dimension. This suggest that stochastic volatility improves extrapolation and interpolation performance in the maturity dimension.

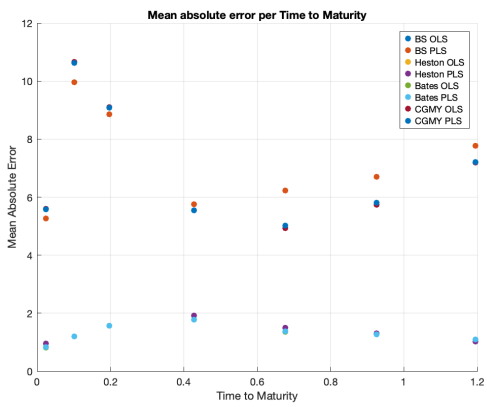

Figure 21: Mean absolute errors in the maturity dimension

Observing the mean absolute error in the strike dimension, see Figure 22, it is clear that the largest errors occur at strike 680. Since all the models exhibit a large mean absolute error at this strike. This is most likely not anything model-specific but rather something systematic. Possible reasons for this could be lower liquidity for this strike or volatility skews. For the most part the Heston and Bates models perform better in the strike dimension, which is clear by observing their lower MAE. At low strikes the Black & Scholes and CGMY models perform similarly well as the Heston and Bates models but for higher strikes the Black & Scholes and CGMY exhibit higher mean absolute errors than the other models. This suggests that the inclusion of stochastic volatility improves performance for higher strikes.

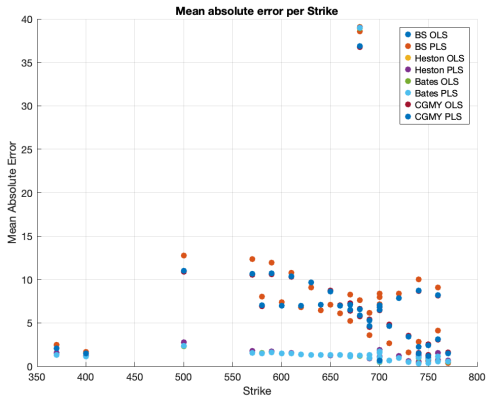

Figure 22: Mean absolute errors in the strike dimension

Analyzing the different models in the different dimensions, it is clear that the Heston and Bates models perform better than the Black & Scholes and CGMY models. The Heston and Bates models make good models since they minimize the errors. The Heston model, characterized by a simpler structure and fewer parameters to estimate than the Bates model, demonstrates performance comparable to the Bates model. Consequently, the Heston model is generally preferable, as simplicity is advantageous in model selection.

3 Portfolio Optimization

In this section of the project, the aim is to solve the Markowitz mean variance portfolio allocation problem below for 12 different assets spanning from stocks to cryptocurrencies to commodity futures.

$$\max_{\omega \in \Omega} \mu^T \omega - \frac{\gamma}{2} \omega^T \Sigma \omega \quad \text{s.t } \mathbf{1}^T \omega = 1$$

In the problem, ω is the relative portfolio weight vector, μ is the conditional expected value vector, Σ is the conditional covariance matrix and Ω is the set of feasible strategies. Further, the weights in ω are constrained to $\omega \geq 0$ as short-selling is not considered to belong to the realm of feasible strategies as it typically adds complexity through extra costs and other complications.

The assets available for the portfolio optimization problem are: Vanguard Total Bond Market Index Fund (BND), Bitcoin USD Price (BTC-USD), Intel Corporation (INTC), Coffee futures (KC=F), NextEra Energy, Inc. (NEE), NVIDIA Corporation (NVDA), Silver futures (SI=F), Sysco Corporation (SYY), UnitedHealth Group Incorporated (UNH), Walmart Inc. (WMT), and Exxon Mobil Corporation (XOM).

An initial budget of 1,000,000 units is set in order to simplify calculations and make an initial allocation. Further, it will be assumed that there are no dividends and that all portfolios are self-financing.

3.1 Start-Up

First, the provided data sets were examined. It was found that a value was missing from the coffee futures (the value of ASSETS(462,5)). To fill this gap, the value was sourced and 154.65 was inserted into the vector (Yahoo Finance 2026).

Further, the returns of all the assets were visualized and displayed in Figure 23. The unconditional mean and variance for each asset and unconditional covariance and correlation were also calculated. The means can be seen in Table 3 and the correlation matrix can be seen in Figure 24.

It is clear that Bitcoin has the highest mean return, followed by NVIDIA. These assets have the highest variances as well, in line with the risk–return tradeoff. Multiple assets have negative mean returns.

There are many assets that show moderate correlation up to almost 0.4, for example NVIDIA and Intel or Exxon and Allstate. The correlation table contains much more positive correlation than negative correlation, making it harder to diversify and highlighting the importance of keeping the covariance structure in mind when investing.

Further, it can be said that the returns appear to be stationary from the plots. This is important for the statistical processes that will be conducted.

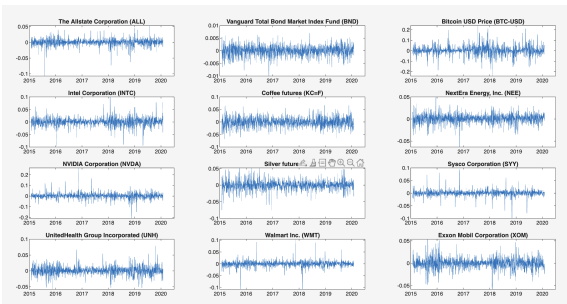

Figure 23: Log returns of assets

3.2 Investment Horizon

The investment horizon is defined at a monthly frequency, meaning that returns are measured and portfolios are rebalanced on a monthly basis. This choice is appropriate given the focus on strategic

Table 3: Unconditional Mean Returns and Variances of Assets

Asset	**Mean**	**Variance**
The Allstate Corporation (ALL)	0.000408	0.010939
Vanguard Total Bond Market Index Fund (BND)	0.000010	0.002076
Bitcoin USD Price (BTC-USD)	0.002928	0.044365
Intel Corporation (INTC)	0.000548	0.016312
Coffee Futures (KC=F)	-0.000372	0.018622
NextEra Energy, Inc. (NEE)	0.000702	0.010206
NVIDIA Corporation (NVDA)	0.002029	0.026663
Silver Futures (SI=F)	-0.000030	0.013786
Sysco Corporation (SYY)	0.000575	0.011444
UnitedHealth Group Incorporated (UNH)	0.000770	0.013631
Walmart Inc. (WMT)	0.000234	0.012277
Exxon Mobil Corporation (XOM)	-0.000245	0.012026

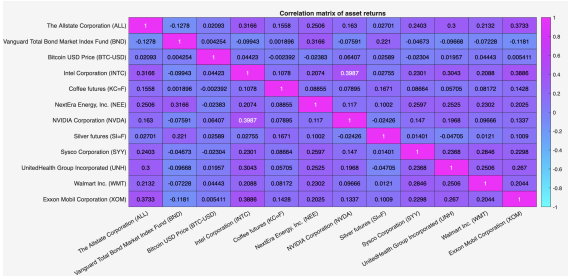

Figure 24: The correlation matrix of the log returns of the assets

asset allocation rather than high-frequency trading. Using monthly returns reduces the impact of market microstructure noise and short-term volatility, and leads to more stable estimates of means and covariances.

Additionally, the monthly investment horizon will be compared to a one-period allocation and a yearly reallocation based on the optimal weighting at the start of the investment period to provide a baseline to compare the continuous trading to.

3.3 Distributions

The empirical distributions of the asset returns were examined using the training sample. For each asset, returns were first demeaned by subtracting the sample mean in order to focus on distributional shape rather than location. The resulting series were then fitted with both a Gaussian distribution and a Student-t location–scale distribution.

To assess the relative fit of the two distributions, maximum likelihood estimation was used and the corresponding log-likelihood values were computed. Figure 25 shows, for each asset, a histogram of the demeaned returns together with the fitted probability density functions of the Normal and Student-t distributions.

The Student-t distribution consistently delivers higher log-likelihood values than the Gaussian distribution across all assets, which indicates a better fit to the empirical return data. This improvement reflects the presence of excess kurtosis and heavier tails in asset returns, which are not captured by the Normal distribution.

Moreover, the figure shows that the Student-t distribution manages to capture the distribution well, indicating that there is no need to consider other distributions. Based on this evidence, the Student-t distribution is considered an appropriate parametric model for the return innovations. This is not surprising as financial data typically inhibits traits like heavy tails.

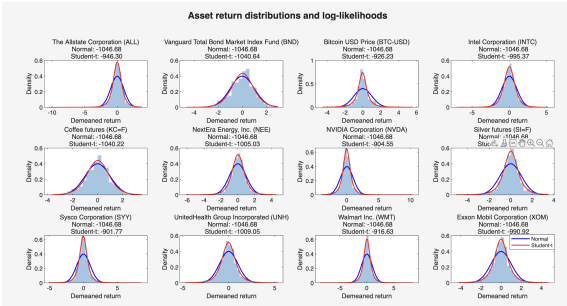

Figure 25: Asset return residuals distributions and their log-likelihoods compared to Normal and Student-t distributions

3.4 Estimating Risk Aversion

The risk aversion parameter, γ, impacts the risk-penalty. A high value will represent a more conservative investor who favors diversification and/or safe assets, and a low value will represent a more aggressive investor prioritizing the expected return.

The range $[1, 50]$ is what is typically considered empirically for the risk aversion parameter, so this interval will be the main focus in determining an appropriate risk aversion parameter for this portfolio allocation problem (Bodnar et al. 2018).

For this assignment, it will be assumed that the agent prefers at least some degree of diversity, so γ will be set to a value that implies moderate diversification of the portfolio based on the unconditional return moments.

As an initial approach, a theoretical calibration method based on elliptical return distributions was used. Under the assumption that asset returns follow an elliptical distribution, mean-variance preferences imply that portfolio weights are invariant up to scale with respect to the risk aversion parameter, and γ can be identified by matching the implied diversification level of the optimal portfolio to a target confidence level. This approach has been proposed in the literature as a theoretically consistent way of calibrating risk aversion when returns are elliptically distributed (Bodnar et al. 2018). Given the distributional analysis in Section 3.3, where ellipticity was found to be a reasonable approximation for the asset returns, this method was deemed appropriate in principle.

The method gave a value of 0.99, which is lower than the interval typically considered. This value gives portfolio weights that are almost fully concentrated to Bitcoin based on the initial allocation. As this was unsuitable given the assumptions, a more empirical method was employed instead.

This more empirical method consisted of viewing the different initial allocations across a grid of γ-values in the mentioned interval. This can be seen in Figure 26. There were many choices with a spread in the allocation that could be reasonable. However, it was noted that two different assets dominated heavily in each of the tails. The risk aversion parameter was then arbitrarily selected at the intersection of those weights, which happened to be at $\gamma = 19$, which gave a reasonable allocation with a spread of many assets that could be considered quite risk averse.

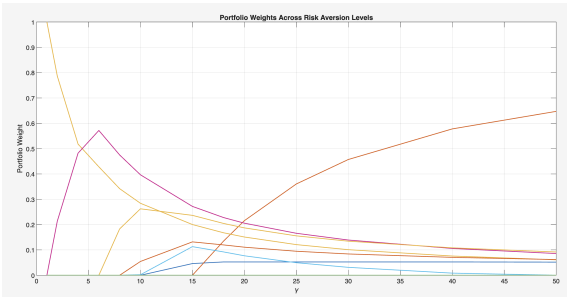

Figure 26: Portfolio weights over a range of γ based on the unconditional moments

3.5 Statistical Modeling

The returns can be described by $r_t = \mu_t + \Sigma^{1/2} z_t$ where z_t follows a Student-t distribution with an elliptical dependence structure. The values for μ_t and Σ can be estimated in many different ways though, and a handful of them will be tested below. These include frameworks like using the unconditional mean and covariance, estimating the conditional mean through AR-processes and estimating the conditional variance through a CCC-GARCH model. Additionally, a DCC-GARCH model with Gaussian innovations is fitted.

3.5.1 Static Model

The static model provides a buy-and-hold benchmark as it calculates the optimal portfolio weights based on the unconditional moments over the training period and allocates the wallet accordingly in the beginning of the testing period. These assets are then held from the end of the training period to the end of the testing period.

As the other models rely on shorter investment horizons, a version of the static model will be adjusted for this as well. This will be done by re-estimating the unconditional means and covariances at each reallocation step, ie monthly or yearly, and implementing a naive predictor. They will, thus, be based on all data up to the current time stamp as opposed to up to the testing period. The optimal weights will then be calculated at the time step and the shares are allocated accordingly from the portfolio value at the time. These values will provide another benchmark for the conditional models.

The portfolio weights for the monthly reallocation and unconditional estimates can be seen in Figure 27.

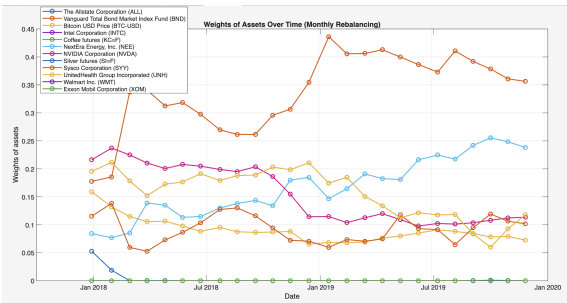

Figure 27: Portfolio weights over the testing period of the model with unconditional mean and covariance and monthly rebalancing

3.5.2 Rolling window

Financial return processes are usually not stationary and the characteristics change over time. Therefore, updating the variance and mean frequent is beneficial. A simple and effective method to implement such updates is through the use of a rolling window approach. By focusing on the most recent data, rolling windows adapt to changes in market conditions, allowing portfolio strategies to respond to shifts in volatility .

The rolling window approach was implemented by updating variance and mean monthly and yearly. Figure 28 illustrates the asset weights each month for the monthly rolling window. It is interesting to observe that the NextEra Energy weight is increasing steadily while most of the others are decreasing.

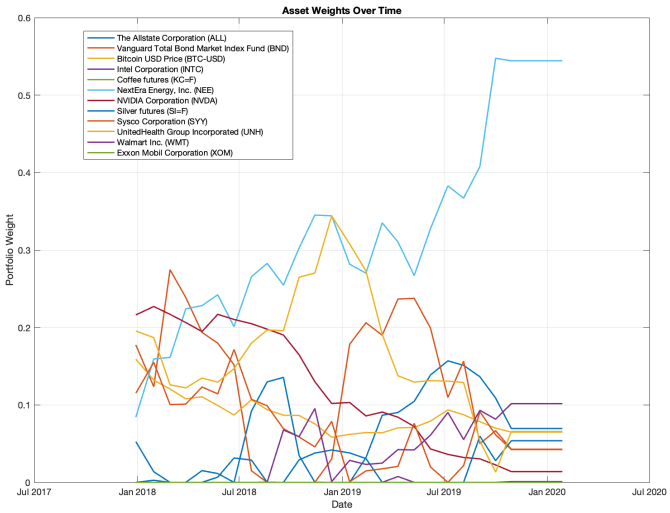

Figure 28: Portfolio weights over the testing period of the model using a rolling window with monthly rebalancing

3.5.3 Conditional Mean Modeling

To expand the framework from the unconditional mean, the conditional mean, $\mu_t = \mathrm{E}[r_t|\mathcal{F}_{t-1}]$, must be modeled.

It was determined that the model should be as simple as possible, so the autocorrelation and partial autocorrelation functions were analyzed in order to determine the simplest model appropriate for modeling each asset. These can be seen in Figure 29 and Figure 30.

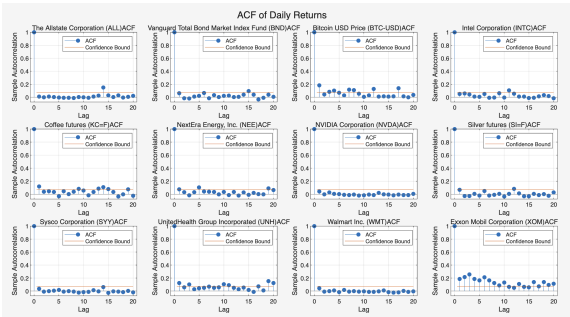

Figure 29: ACF of each asset over the training period

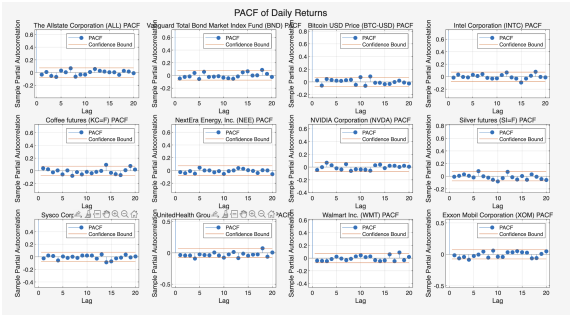

Figure 30: PACF of each asset over the training period

First, the demeaned returns of the training data were tested with a Ljung-Box test at $\alpha = 0.05$ in order to identify the assets that should not be modeled by a more complicated framework than the naive predictor, $\mu_t = \mu_{t-1}$ described by the unconditional estimate at time t. These assets were:

- The Allstate Corporation (ALL)
- Vanguard Total Bond Market Index Fund (BND)
- Bitcoin USD Price (BTC-USD)
- Intel Corporation (INTC)
- NextEra Energy, Inc. (NEE)
- NVIDIA Corporation (NVDA)
- Silver futures (SI=F)
- Sysco Corporation (SYY)
- UnitedHealth Group Incorporated (UNH)
- Walmart Inc. (WMT)

The only assets that do not pass the test are the coffee futures (KC=F) and Exxon Mobil Corporation (XOM). Thus, these two assets need to be modeled continuously.

Exxon Mobil appears to have a decaying autocorrelation-function and no strong MA-structure in the PACF. This indicates that an AR-model may be appropriate. As an AR(1)-model did not pass the Ljung-Box test more complicated models such as an AR(2) and ARMA(1,1) were tested. These did not either pass the Ljung-Box test. However, the AR(3)-model did pass the test. This was regarded as an appropriate model considering the ACF and PACF as well. However, a control was made to ensure that the model does not overfit the data. The AR(3) amounted to a modest increase in the BIC and AIC, but because the fit to the Ljung-Box test was much greater it was still selected. The values can be seen in Table 4.

Table 4: Model comparisons for the conditional mean of Exxon Mobil (XOM)

AR order p	AIC	BIC	Ljung–Box p-value
1	-4490.8	-4477.0	0.0203
2	-4491.8	-4473.4	0.0449
3	-4491.1	-4468.1	0.0886

The estimated AR(3)-process for Exxon Mobil is $r_t^{demeaned} = -0.0196\, r_{t-1} - 0.0632\, r_{t-2} - 0.0420\, r_{t-3} + \varepsilon_t$.

Commodity futures can be messier to model than stocks, as things like the Coffee Future can vary with the season or other exogenous factors. However, nothing special sticks out in Figure 23 or in the ACF and PACF. Thus, this asset will be approached in the same way as Exxon Mobil by starting as simple as possible and then expanding the model and controlling for overfitting.

Thus, several different models including AR(1), AR(2), AR(3) and ARMA(1,1) were tested. The results, which can be seen in Table 5, indicate that an AR(1) model is sufficient.

Table 5: Model comparison for the conditional mean of Coffee Futures (KC=F)

ARMA order p	AIC	BIC	Ljung–Box p-value
(1,0)	-3796.18	-3782.37	0.0794
(2,0)	-3794.69	-3776.28	0.0915
(3,0)	-3793.05	-3770.03	0.1262
(1,1)	-3796.37	-3777.95	0.0692

The estimated AR(1)-process for Coffee Futures is $r_t^{demeaned} = 0.03886 r_{t-1} + \varepsilon_t$.

3.5.4 Constant Conditional Correlation-GARCH with Gaussian Innovations

To improve predictive performance beyond an unconditional variance–covariance specification, the conditional dependence structure of returns was modeled using a multivariate Constant Conditional Correlation GARCH (CCC–GARCH) framework. The CCC–GARCH model combines univariate GARCH processes for individual asset variances with a time-invariant correlation matrix governing cross-asset dependence.

The CCC–GARCH framework offers a convenient compromise between model flexibility and practical feasibility. By allowing conditional variances to vary over time while keeping correlations fixed, the model is able to capture volatility clustering and cross-sectional dependence without the substantial increase in dimensionality and estimation complexity that fully dynamic multivariate volatility models often entail. This makes CCC–GARCH well suited for portfolios containing a moderate number of assets. Depending on the empirical adequacy of the constant-correlation assumption, assessed through residual diagnostics and goodness-of-fit measures, the model can be extended to a Dynamic Conditional Correlation (DCC-GARCH) framework to allow correlations to evolve over time and capture additional predictive structure.

The model assumes $\varepsilon_t = \mathbf{H}_t^{1/2}\mathbf{z}_t,\ \mathbf{z}_t \sim \mathcal{N}(\mathbf{0}, \mathbf{I})$, where ε_t denotes the vector of demeaned asset returns at time t and the conditional covariance matrix is decomposed as $\mathbf{H}_t = \mathbf{D}_t\mathbf{R}\mathbf{D}_t$.

Here, $\mathbf{D}_t = \mathrm{diag}(\sqrt{h_{1,t}}, \ldots, \sqrt{h_{N,t}})$ contains the conditional standard deviations, and $\mathbf{R}$ is a constant correlation matrix.

Each conditional variance follows a univariate GARCH(1,1) process,

$$h_{i,t} = \omega_i + \alpha_i \varepsilon_{i,t-1}^2 + \beta_i h_{i,t-1}, \qquad i = 1, \ldots, N,$$

which is a specification that has been shown to be difficult to outperform empirically and therefore serves as a robust baseline for volatility modeling. These values are used for the forecast in order to optimize the portfolio at the relevant time steps.

Model parameters were estimated by maximum likelihood, assuming conditionally Gaussian innovations. The corresponding log-likelihood function is given by:

$$\ell = -\frac{1}{2}\sum_{t=1}^{T}\left[N\ln(2\pi) + \ln(|H_t|) + \varepsilon_t' H_t^{-1}\varepsilon_t\right]$$

Figure 31 displays the estimated conditional log-volatilities for each asset in the training sample. The pronounced time variation and clustering confirm that the CCC–GARCH model successfully captures the dominant volatility dynamics present in the data.

Figure 31: Estimated conditional log-volatilities from the CCC-GARCH model with Gaussian innovations

To assess the adequacy of the Gaussian CCC–GARCH specification, standardized residuals were constructed and decorrelated using the Cholesky factor of the estimated correlation matrix. Under the correct model specification, these residuals should be independent and identically distributed standard normal variables. First, the excess kurtosis of the decorrelated residuals was examined and found to be predominantly positive, indicating heavier tails than the Gaussian distribution

implies. Second, the quadratic form $q_t = \mathbf{u}_t'\mathbf{u}_t$, where $\mathbf{u}_t$ denotes the decorrelated standardized residuals, was compared to the theoretical χ^2_N distribution, as can be seen in Figure 32. The systematic deviations from the 45° line, indicate that the tails should be thicker than the Gaussian model can capture.

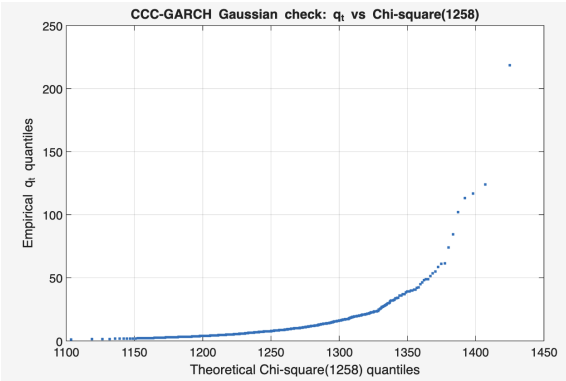

Figure 32: Q-Q plot of the quadratic form of decorrelated standardized residuals from the Gaussian CCC–GARCH model against the theoretical χ^2_N distribution

These results suggest that while the Gaussian CCC–GARCH model captures volatility clustering and dependence structure reasonably well, it fails to adequately model the tail behavior of the joint return distribution. This motivates extending the model to allow for heavy-tailed innovations, which is addressed in the following section through a CCC–GARCH model with Student-t distributed errors.

The portfolio weights over the testing period assuming monthly reallocations using CCC-GARCH with Gaussian innovations and assuming the unconditional mean can be observed in Figure 33. Figure 34 shows the weights with the conditional mean estimation instead.

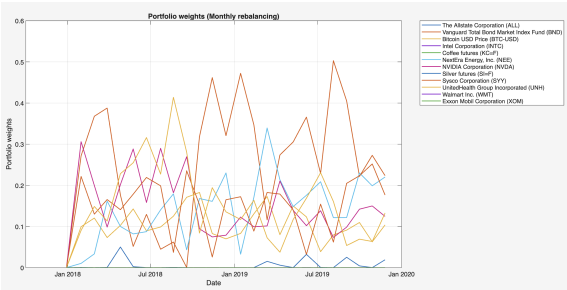

Figure 33: Portfolio weights over the testing period of the model using a CCC-GARCH with Gaussian innovations and the unconditional mean estimate with monthly rebalancing

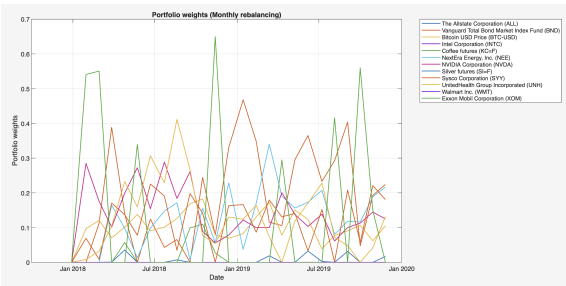

Figure 34: Portfolio weights over the testing period of the model using a CCC-GARCH with Gaussian innovations and the conditional mean estimate with monthly rebalancing

3.5.5 Constant Conditional Correlation-GARCH with Student-t Innovations

To address the limitations of the CCC-GARCH with Gaussian innovations, the framework is extended by allowing the standardized innovations to follow a multivariate Student-t distribution. This modification preserves the overall structure of the model while introducing heavier tails through an additional degrees-of-freedom parameter, ν. As a result, extreme return realizations can be accommodated more naturally, something that is particularly important in financial return data.

The conditional covariance matrix is still decomposed as $\mathbf{H}_t = \mathbf{D}_t \mathbf{R} \mathbf{D}_t$, where $\mathbf{D}_t$ contains the conditional standard deviations governed by univariate GARCH(1,1) dynamics, and $\mathbf{R}$ is a constant correlation matrix.

Under the Student-t assumption, the log-likelihood function becomes

$$\ell = \sum_{t=1}^{T} \left[\ln \Gamma\left(\frac{\nu+N}{2}\right) - \ln \Gamma\left(\frac{\nu}{2}\right) - \frac{N}{2}\ln(\nu\pi) - \frac{1}{2}\ln(|H_t|) - \frac{\nu+N}{2}\ln\left(1 + \frac{1}{\nu}\varepsilon_t' H_t^{-1}\varepsilon_t\right)\right]$$

where $\nu > 2$ controls the thickness of the tails. As $\nu \to \infty$, the Student-t distribution converges to the Gaussian case, making the Gaussian CCC–GARCH a nested case of this specification.

The estimated conditional volatilities from the Student-t CCC–GARCH model are shown in Figure 35. Overall, the volatility dynamics closely resemble those obtained under Gaussian innovations, suggesting that the underlying variance behavior is largely unaffected by the choice of distribution. The primary distinction arises in the treatment of extreme observations, which are handled more flexibly under the Student-t specification.

To test the fit of the Student-t distribution in the CCC-GARCH, univariate Q-Q plots of decorrelated standardized residuals were plotted against a Student-t distribution with the estimated degrees of freedom (8), as can be seen in Figure 36. These plots show a close agreement across most of the assets, supporting the use of Student-t with the CCC-GARCH framework.

Figures 37 and 38 display the evolution of portfolio weights under monthly rebalancing, using both unconditional and conditional mean specifications.

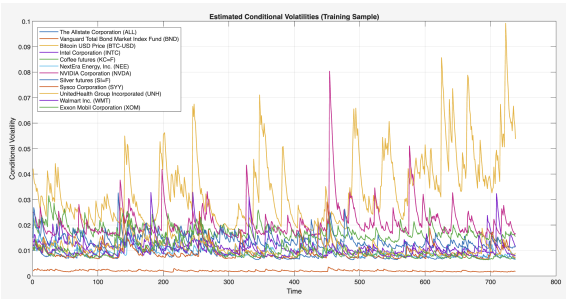

Figure 35: Estimated conditional volatilites from the CCC-GARCH model with Student-t innovations over the training period

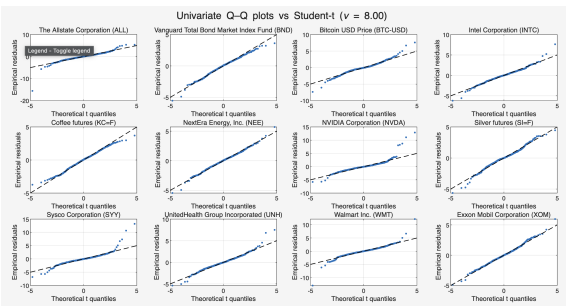

Figure 36: Q-Q plot of decorrelated standardized residuals from the CCC–GARCH model against a Student-t distribution with estimated degrees of freedom $\nu = 8$.

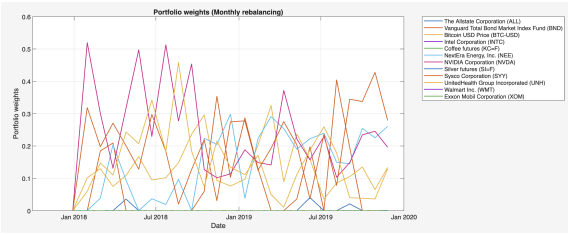

Figure 37: Portfolio weights over the testing period of the model using a CCC-GARCH with Student-t innovations and the unconditional mean estimate with monthly rebalancing

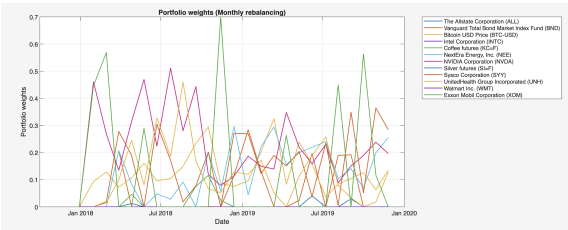

Figure 38: Portfolio weights over the testing period of the model using a CCC-GARCH with Student-t innovations and the conditional mean estimate with monthly rebalancing

3.5.6 Dynamic Conditional Correlation-GARCH for Conditional Covariances with Gaussian Distribution

To expand the CCC-GARCH framework, the conditional covariance matrix is modeled using a Dynamic Conditional Correlation GARCH (DCC-GARCH) specification. This is implemented through the DCC framework of Engle and Sheppard where the conditional covariance matrix is decomposed into time-varying standard deviations and a time-varying correlation matrix (Engle and Sheppard 2001).

Let $x_t \in \mathbb{R}^N$ denote the demeaned return vector. The model is:

$$x_t \mid \mathcal{F}_{t-1} \sim \mathcal{N}(0, H_t), \qquad H_t = D_t R_t D_t, \tag{8}$$

where $D_t = \mathrm{diag}(\sqrt{h_{1t}}, \ldots, \sqrt{h_{Nt}})$ and R_t is the conditional correlation matrix.

Each asset variance is modeled as $h_{it} = \omega_i + \alpha_i x_{i,t-1}^2 + \beta_i h_{i,t-1}$, with $i = 1, \ldots, N$, and the standard positivity and stationarity-type restrictions $\omega_i > 0$, $\alpha_i \geq 0$, $\beta_i \geq 0$ and $\alpha_i + \beta_i < 1$.

Time variation in the conditional correlations is captured by a positive definite matrix Q_t described by:

$$Q_t = (1 - a - b)\,\bar{Q} + a\,\varepsilon_{t-1}\varepsilon_{t-1}^\top + b\,Q_{t-1}, \tag{9}$$

$$R_t = Q_t^{*\,-1} Q_t Q_t^{*\,-1}, \tag{10}$$

where $\bar{Q}$ is the unconditional covariance matrix of standardized residuals, and $Q_t^* = \mathrm{diag}(\sqrt{q_{11,t}}, \ldots, \sqrt{q_{NN,t}})$. $\bar{Q}$ is estimated by the sample moment $\bar{Q} = \frac{1}{T}\sum_{t=1}^{T} \varepsilon_t \varepsilon_t^\top = \frac{\varepsilon^\top \varepsilon}{T}$. (Song 2009)

Under conditional multivariate normality, the log-likelihood can be written as

$$L = -\frac{1}{2}\sum_{t=1}^{T}\left(k\log(2\pi) + 2\log|D_t| + \log|R_t| + \varepsilon_t' R_t^{-1}\varepsilon_t\right), \tag{11}$$

To enforce the constraints $a \geq 0$, $b \geq 0$, and $a + b < 1$ during unconstrained numerical optimization, the code maps unconstrained scalars $(\tilde{a}, \tilde{b}) \in \mathbb{R}^2$ into (a, b) through a softmax-type transform:

$$a = \frac{e^{\tilde{a}}}{1 + e^{\tilde{a}} + e^{\tilde{b}}} \qquad b = \frac{e^{\tilde{b}}}{1 + e^{\tilde{a}} + e^{\tilde{b}}},$$

guaranteeing $a > 0$, $b > 0$, and $a + b < 1$ by construction. The same idea is applied elementwise to (α_i, β_i) through $(\tilde{\alpha}_i, \tilde{\beta}_i)$ to ensure $\alpha_i, \beta_i \geq 0$ and $\alpha_i + \beta_i < 1$ for each asset.

The portfolio weights for the portfolio rebalanced monthly with DCC can be seen in Figures 39 and 40 with the unconditional mean and the conditional mean, respectively.

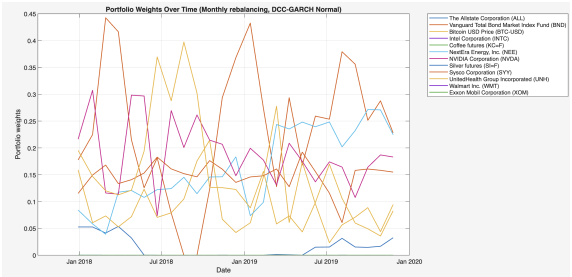

Figure 39: DCC GARCH weights Gaussian innovations unconditional mean Portfolio weights over the testing period of the model using a DCC-GARCH with Gaussian innovations and the unconditional mean estimate with monthly rebalancing

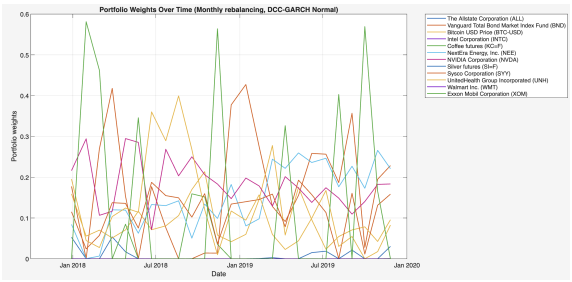

Figure 40: DCC GARCH weights Gaussian innovations unconditional mean Portfolio weights over the testing period of the model using a DCC-GARCH with Gaussian innovations and the conditional mean estimate with monthly rebalancing

3.6 Choice of Performance Metrics

As all portfolio strategies are evaluated over the same out-of-sample testing period, model performance can be compared directly using simple portfolio returns over the full horizon. There is therefore no need to geometrically normalize returns across models, and total return provides a transparent measure of overall profitability.

The metrics from Kolari, Liu, and Pynnönen 2024 were considered, and it was determined that the Sharpe Ratio and Value-at-Risk would be evaluated alongside the portfolio return in order to assess the models.

To complement total return and capture different dimensions of portfolio performance, additional risk-adjusted and downside-risk measures were selected. Following the discussion in Kolari, Liu, and Pynnönen 2024, the Sharpe ratio and Value-at-Risk (VaR) were chosen as the primary risk metrics. Together, these measures provide a balanced assessment of return, variability, and tail risk, which is consistent with the objectives of the assignment.

3.6.1 Sharpe Ratio

The Sharpe ratio measures the excess return per unit of risk and is defined as

$$\mathrm{sr}_P = \frac{\mathbb{E}(r_P) - r_f}{\sigma_P}$$

where r_P denotes the portfolio return, r_f is the risk-free rate, and σ_P is the standard deviation of portfolio returns.

For simplicity, the risk-free rate is assumed to be constant over the testing period and is set to $r_f = 0.045$ annually, based on average estimates for a similar time period (Anwar, Dewi, and Natsir 2023). While this is a very simplifying assumption, it is sufficient for the purpose of relative model comparison, which is the primary objective of this analysis.

Sharpe ratios were computed using returns at the rebalancing frequency implied by each strategy. For portfolios with monthly rebalancing, annual Sharpe ratios were constructed by aggregating monthly portfolio values into annual returns, ensuring consistency across models. Due to the limited number of annual observations, the resulting variance estimates can be unstable. The Sharpe ratio should therefore be interpreted as an indicative measure of risk-adjusted performance rather than a precise statistical estimate.

3.6.2 Value-at-Risk

To assess downside risk, Value-at-Risk (VaR) at the 95% confidence level was also computed. VaR summarizes the magnitude of potential losses in the lower tail of the return distribution and provides information that is not captured by variance-based measures.

VaR is estimated using the empirical (historical) distribution of portfolio returns. Let $\{r_{P,t}\}_{t=1}^{T}$ denote the sequence of monthly portfolio returns over the testing period. The 95% Value-at-Risk is then defined as

$$\mathrm{VaR}_{0.95} = -\inf\left\{x \in \mathbb{R} \,:\, \mathbb{P}(r_{P,t} \leq x) \geq 0.05\right\},$$

which in practice corresponds to the negative 5th empirical quantile of the return distribution. The VaR is computed as $\mathrm{VaR}_{0.95} = -Q_{0.05}(r_P)$ where $Q_{0.05}$ denotes the 5th sample quantile. It can be interpreted as in the worst 5% of months, the portfolio is expected to lose at least $\mathrm{VaR}_{95\%}$ percent of its value.

VaR is evaluated at the monthly horizon, which aligns with the portfolio rebalancing frequency and provides a sufficient number of observations for reliable estimation. Computing VaR at an annual frequency was avoided, as the limited number of annual observations would render tail quantile estimates unreliable.

3.7 Results

The portfolio return over the testing period for each of the models and their respective annualized Sharpe ratios can be seen in Table 6. The Value-at-Risk values for the models with monthly rebalancing can be seen in Table 7.

Table 6: Out-of-sample performance comparison across models and investment horizons without transactions costs

Model	Horizon	Total return(%)	Annual Sharpe ratio (%)
Unconditional Markowitz	Static	17.69	–
Unconditional Markowitz	Annually	12.29	4.69
Unconditional Markowitz	Monthly	17.89	13.40
Rolling Window	Annually	18.21	7.9
Rolling Window	Monthly	22.02	14.12
CCC-GARCH Constant Mean + Normal Distribution	Annually	8.89	-1.02
CCC-GARCH Constant Mean + Normal Distribution	Monthly	33.88	30.41
CCC-GARCH Constant Mean + Student-t Distribution	Annually	15.17	8.85
CCC-GARCH Constant Mean + Student-t Distribution	Monthly	47.35	35.87
CCC-GARCH Cond. Mean + Normal Distribution	Annually	8.75	-1.26
CCC-GARCH Cond. Mean + Normal Distribution	Monthly	18.22	8.25
CCC-GARCH Cond. Mean + Student-t Distribution	Annually	15.00	8.63
CCC-GARCH Cond. Mean + Student-t Distribution	Monthly	30.82	22.93
DCC-GARCH Constant Mean + Normal Distribution	Annually	12.28	4.49
DCC-GARCH Constant Mean + Normal Distribution	Monthly	40.31	36.38
DCC-GARCH Cond. Mean + Normal Distribution	Annually	12.54	4.89
DCC-GARCH Cond. Mean + Normal Distribution	Monthly	27.19	23.02

Table 7: Out-of-sample risk comparison across models and investment horizons without transaction costs

Model	$\text{VaR}_{95\%}$ (%)
Unconditional Markowitz	5.24
Rolling Window	4.03
CCC-GARCH Constant Mean + Normal Distribution	4.76
CCC-GARCH Constant Mean + Student-t Distribution	5.91
CCC-GARCH Cond. Mean + Normal Distribution	6.65
CCC-GARCH Cond. Mean + Student-t Distribution	7.24
DCC-GARCH Constant Mean + Normal Distribution	5.83
DCC-GARCH Cond. Mean + Normal Distribution	7.82

The highest total return over the period belongs to the CCC-GARCH with Student-t innovations and the unconditional mean rebalanced monthly. The largest Sharpe ratio, however, belongs to the DCC-GARCH with constant mean and normally distributed innovations. The lowest Value-at-Risk belongs to the rolling window.

3.7.1 Unconditional Covariance

Figure 41 shows the portfolio value obtained using unconditional mean and covariance estimates with monthly rebalancing. The portfolio exhibits a moderate upward trend over the testing period, with some pronounced drawdowns, particularly during periods of increased market volatility.

Since the covariance matrix is estimated using unconditional moments, the model does not adapt to changing volatility conditions over time. As a result, the portfolio reacts more slowly to shifts in risk, leading to larger temporary losses during turbulent periods and slower recoveries compared to volatility-based models. However, the overall positive performance indicates that periodic rebalancing alone provides some risk control, even in the absence of dynamic volatility modeling.

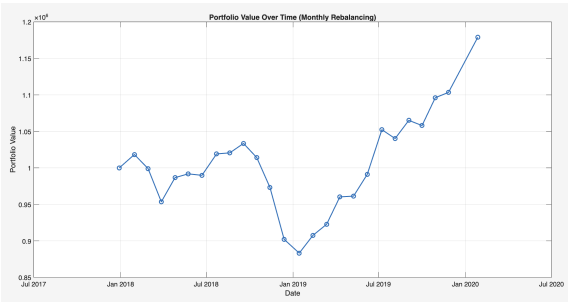

Figure 41: Portfolio value of the unconditional estimates with monthly rebalancing

3.7.2 Rolling Window

Figures 42 and 43 illustrates the portfolio value using rolling window with yearly and monthly rebalancing. Not including the transaction costs gave a overall increase in portfolio value, with some dips for the monthly rebalancing. More frequent recalculating of the weights gave higher portfolio value in the end, if transaction costs were not included.

Inclusion of transaction costs significantly worsened the portfolio value for the monthly rebalancing, where the final portfolio value was lower than the initial portfolio value. For the yearly rebalancing the transaction costs decreased the final portfolio value a bit but the final value still stayed higher than the initial.

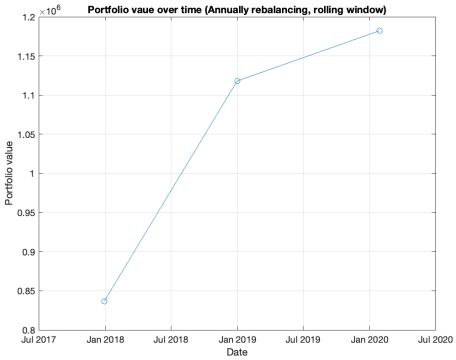

(a) Portfolio value with rolling window without transaction costs

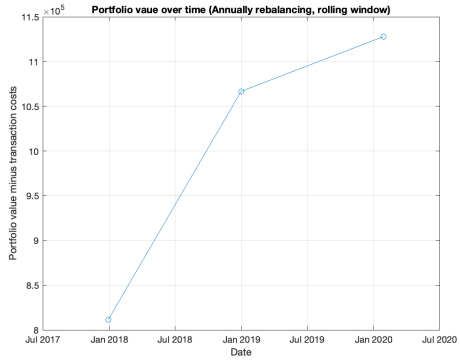

(b) Portfolio value with rolling window with transaction costs

Figure 42: Portfolio value with rolling window with and without transaction costs

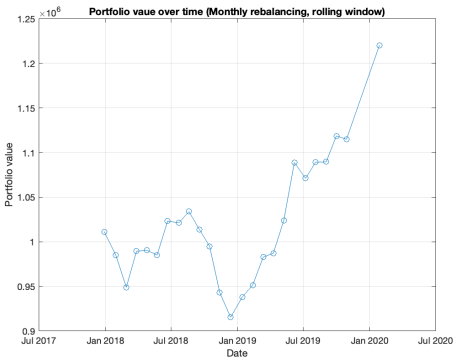

(a) Portfolio value with rolling window without transaction costs

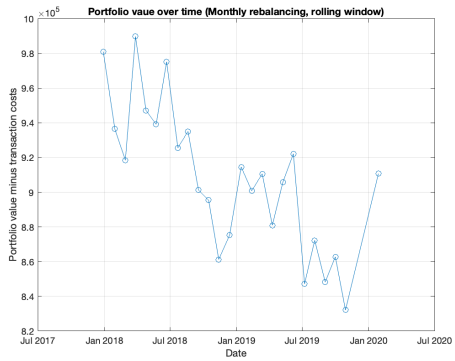

(b) Portfolio value with rolling window with transaction costs

Figure 43: Portfolio value with rolling window with and without transaction costs

3.7.3 CCC-GARCH

Figures 44-47 illustrate the evolution of portfolio values with CCC-GARCH covariance modeling combined with different distributions and modeling of the mean with monthly rebalancing.

Figure 44 shows the portfolio value obtained using CCC-GARCH with Gaussian innovations and an unconditional mean. The portfolio exhibits a generally upward trend over the testing period, but with noticeable drawdowns and periods of stagnation. This behavior reflects the model's ability to adapt to changing volatility through time-varying variances, while the assumption of Gaussian innovations limits its ability to fully capture extreme return realizations.

In Figure 45, the same CCC-GARCH model with Gaussian innovations is combined with a conditional mean specification. Compared to the unconditional mean case, the portfolio path appears more volatile and achieves a lower final value. This suggests that, at the monthly horizon, incorporating a conditional mean adds estimation noise without providing a substantial improvement in predictive power, which is consistent with the relatively weak mean predictability observed in asset returns.

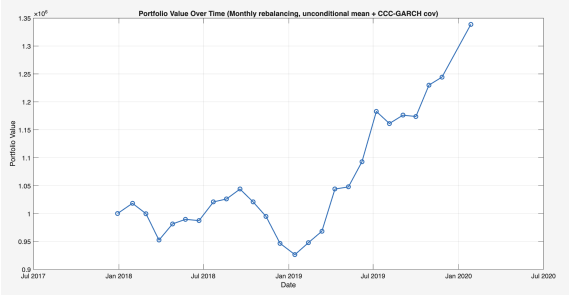

Figure 44: Portfolio value over the testing period with monthly rebalancing using the CCC-GARCH model with Gaussian innovations and an unconditional mean

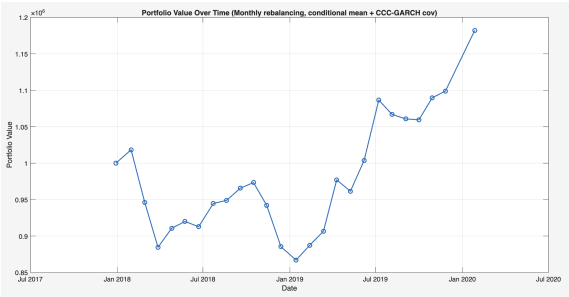

Figure 45: Portfolio value over the testing period with monthly rebalancing using the CCC-GARCH model with Gaussian innovations and a conditional mean

Figure 46 displays the portfolio value under CCC-GARCH with Student-t innovations and a conditional mean. The heavier-tailed Student-t distribution allows the model to better accommodate extreme return observations, resulting in stronger growth during favorable market periods. However, this also leads to sharper drawdowns, indicating increased exposure to tail risk.

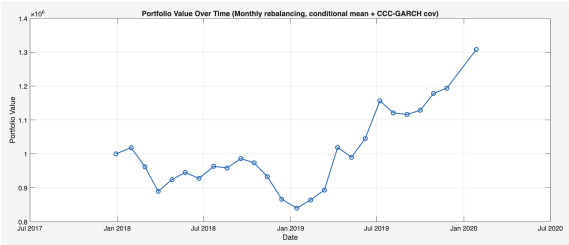

Figure 46: Portfolio value over the testing period with monthly rebalancing using the CCC-GARCH model with Student-t innovations and a conditional mean

Finally, Figure 47 shows the CCC-GARCH model with Student-t innovations and an unconditional mean. This specification yields the strongest overall performance among the CCC-GARCH variants, combining robust growth with relatively stable dynamics. The result highlights the importance of modeling heavy tails in return innovations, while avoiding potentially noisy conditional mean estimates at the monthly frequency.

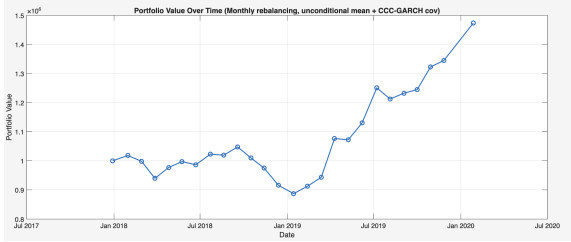

Figure 47: Portfolio value over the testing period with monthly rebalancing using the CCC-GARCH model with Student-t innovations and an unconditional mean

3.7.4 DCC-GARCH

Figure 48 shows the portfolio value over the testing period obtained using the DCC-GARCH model with Gaussian innovations and monthly rebalancing, assuming an unconditional mean. The portfolio starts at the initial investment level and exhibits moderate fluctuations during the early part of the sample, followed by a pronounced decline around the beginning of 2019. After this drawdown, the portfolio recovers steadily and enters a strong upward phase, reaching its highest value toward the end of the testing period. Overall, the portfolio value displays a positive trend over the entire testing horizon.

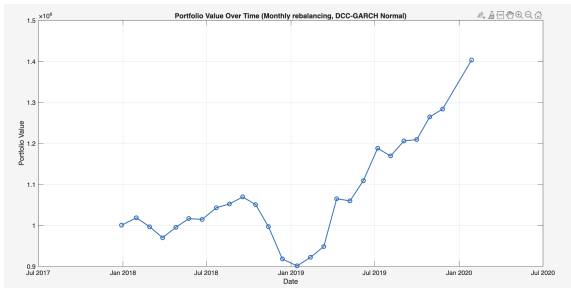

Figure 48: Portfolio value with monthly rebalancing using DCC-GARCH and Gaussian innovations with unconditional mean

Figure 49 presents the corresponding portfolio value when the DCC-GARCH model with Gaussian innovations is combined with a conditional mean specification. The portfolio path follows a similar overall pattern, with noticeable short-term fluctuations and a drawdown around early 2019, followed by a recovery and subsequent growth toward the end of the sample. Compared to the unconditional mean case, the portfolio trajectory appears slightly more volatile, reflecting increased sensitivity to short-term return dynamics.

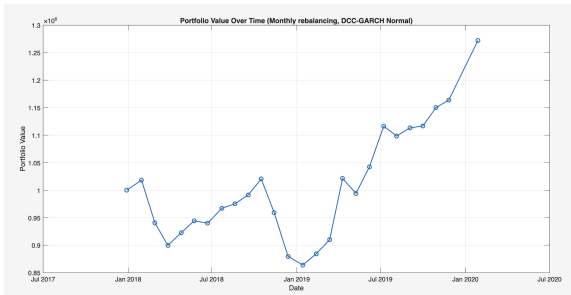

Figure 49: Portfolio value with monthly rebalancing using DCC-GARCH and Gaussian innovations with conditional mean

3.7.5 Analysis and Relative Model Validation

The results in Tables 6 and 7 reveal several clear patterns regarding the impact of covariance modeling, distributional assumptions, and rebalancing frequency on portfolio performance.

First, increasing the rebalancing frequency from annual to monthly consistently improves both total returns and risk-adjusted performance across nearly all models. This effect is particularly pronounced for models that incorporate time-varying covariance structures, such as the rolling window, and GARCH-based approaches. More frequent rebalancing allows the portfolio to react faster to changes in the estimated risk structure to improve capital allocation over time. Notably, none of the portfolios with annual rebalancing outperform the static portfolio, suggesting that annual rebalancing is not an appropriate investment horizon in this setting. These results indicate that more frequent rebalancing, such as bi-weekly, should be considered as they could possibly improve performance further.

Comparing unconditional covariance estimates with rolling window approaches shows that even simple forms of time variation in the covariance matrix lead to performance gains. The rolling window model achieves higher returns and a lower Value-at-Risk than the portfolio with unconditional mean and covariance estimates, indicating improved downside risk control. This suggests that ignoring time variation in second moments leads to worse risk estimates, particularly during volatile periods.

The CCC-GARCH models further improve upon these results in most cases by explicitly modeling conditional heteroskedasticity. Monthly rebalanced CCC-GARCH portfolios consistently outperform their annually rebalanced counterparts, confirming that volatility forecasts are most informative at shorter horizons. The results show a strong sensitivity to the assumed innovation distribution. Across both unconditional and conditional mean specifications, Student-t innovations dominate Gaussian innovations in terms of both total return and Sharpe ratio. This finding is consistent with the presence of heavy tails in asset returns, which the Gaussian assumption fails to capture sufficiently.

The DCC-GARCH results indicate that allowing for time-varying correlations can further improve performance relative to models with constant conditional correlations. In particular, the DCC-GARCH model with an unconditional mean, Gaussian innovations and monthly rebalancing achieves a higher total return and Sharpe ratio than its CCC-GARCH peer, and the highest Sharpe ratio overall. This suggests that capturing dynamic correlation structures provides additional benefits beyond modeling time-varying variances alone. However, a DCC-GARCH combined with Student-t innovations has not been tested due to time constraints. When combined with a conditional mean, the DCC-GARCH model performs worse than the unconditional mean, which is consistent with the findings for the CCC-GARCH models.

Across both CCC-GARCH and DCC-GARCH specifications, incorporating a conditional mean does not lead to systematic performance improvements. In most cases, conditional mean models result in lower returns and higher risk compared to their unconditional counterparts. This indicates that, at the monthly horizon considered, mean return predictability is weak and that estimation error in the conditional mean may outweigh any potential forecasting gains. Instead, modeling higher-order moments such as volatility dynamics, correlation dynamics, and tail behavior appears to be more important for portfolio optimization.

The Value-at-Risk results reinforce these conclusions. Models with heavier-tailed distributions tend to exhibit higher VaR values, reflecting increased exposure to tail risk, even when average performance improves. The rolling window model achieves the lowest VaR among the reported specifications, indicating strong downside protection despite more modest returns. This highlights the trade-off between return maximization and tail risk exposure. However, the VaR is based off very few data points so the results should be interpreted with caution.

Overall, the results demonstrate that allowing for time-varying volatility and correlation structures substantially improves portfolio performance relative to unconditional covariance models. In particular, CCC-GARCH and DCC-GARCH models with monthly rebalancing dominate simpler approaches in terms of both returns and risk-adjusted performance. The consistent outperformance of Student-t innovations in the CCC-GARCH framework further confirms the importance of accounting for heavy tails in financial return modeling.

It is important to emphasize, however, that none of the considered models provides a complete

or fully accurate description of the underlying data-generating process. Each specification relies on simplifying assumptions that are inevitably violated in practice. Still, the results illustrate that some models are more useful than others for portfolio allocation purposes, particularly when they capture key empirical features such as volatility clustering, dynamic correlations, and fat tails. In this sense, the value of a model lies not in its realism, but in its ability to improve decision-making under uncertainty. As famously stated, "all models are wrong, but some are useful". (Wiktorsson 2025a)

Finally, it should be noted that extending the DCC-GARCH framework to incorporate Student-t innovations would be a natural next step. Given the strong performance of Student-t innovations in the CCC-GARCH setting, it is plausible that a DCC-GARCH model with heavy-tailed innovations could further improve both return and risk-adjusted performance. Due to time constraints, this was not implemented in the present project, but it represents an important direction for future research.

3.8 Transaction Costs

The previous results have ignored possible transaction costs. As these costs are very tangible in a real-world setting, it gives a deceptive picture of the optimal portfolio allocation. With transaction costs, the portfolio optimization problem can be written as below instead.

$$\max_{\omega \in \Omega} \mu^T \omega - \frac{\gamma}{2} \omega^T \Sigma \omega - c * |S^T \circ (w - w_0)| \quad \text{s.t } \mathbf{1}^T \omega = 1$$

After transaction costs are added, portfolios are rescaled to remain self-financing. To show the significance of including transaction costs, a rolling window where the weights are updated daily was performed. Figure 50 illustrates the portfolio value using a rolling window and daily rebalancing, with and without transaction costs. In this example, transaction costs of 3% of the prices of the options sold and bought were used. Observing the plots, it is clear that without the transaction costs, the portfolio value is increasing significantly, which can give a false indication that this method is beneficial. Adding the transaction costs into the equation reveals that this method is very costly and the transaction costs outweigh the benefits of frequent rebalancing. This further supports the chosen investment horizons, which are monthly and annually, as they keep the transaction costs down, while still reaping trade benefits. This is closer to a more realistic trading setting as the transaction costs, which were ignored in the previous results, are less relevant.

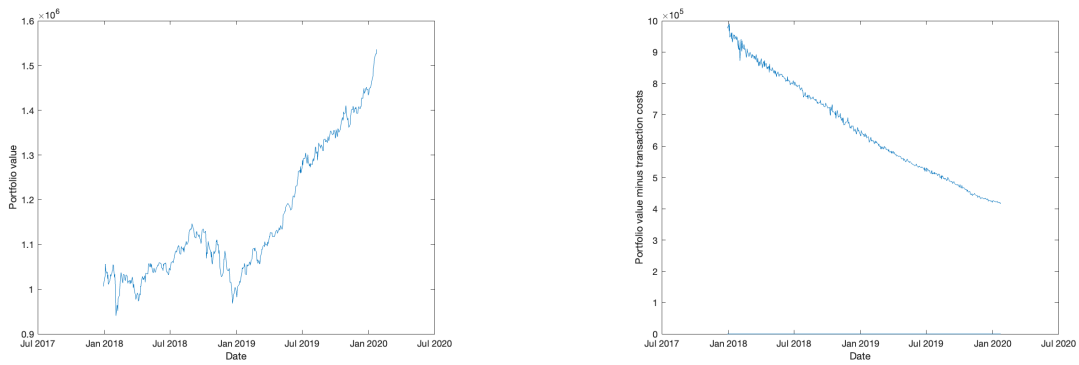

(a) Portfolio value with rolling window without transaction costs

(b) Portfolio value with rolling window with transaction costs

Figure 50: Portfolio value with rolling window with and without transaction costs

References

Anwar, Nurul Rahmah Dewi, and Uhud Darmawan Natsir (2023). "Application of the Capital Asset Pricing Model (CAPM) Method in Determining Efficient Stock Group (Study on IDX30 and Business Index-27 in Indonesia Stock Exchange)". In: *International Journal of Humanities Education and Social Sciences* 2.6, pp. 1734–1848. ISSN: 2808-1765. URL: https://ijhess.com/index.php/ijhess/.

Bates, David S. (1996). "Jumps and stochastic volatility: Exchange rate processes implicit in PHLX Deutsche Mark options". In: *Review of Financial Studies* 9.1, pp. 69–107.

Belomestny, Denis (2011). "Statistical Inference for Time-Changed Lévy Processes via Composite Characteristic Function Estimation". In: *The Annals of Statistics* 39.4, pp. 2205–2242. DOI: 10.1214/11-AOS901.

Bodnar, Taras et al. (2018). "Determination and estimation of risk aversion coefficients". In: *Computational Management Science* 15.3, pp. 297–317. DOI: 10.1007/s10287-018-0317-x.

Carr, Peter et al. (2002). "The Fine Structure of Asset Returns: An Empirical Investigation". In: *Journal of Business* 75.2, pp. 305–332.

Christoffersen, Peter F. (1998). "Evaluating Interval Forecasts". In: *International Economic Review* 39.4, pp. 841–862.

Engle, Robert F. and Kevin Sheppard (2001). *Theoretical and Empirical Properties of Dynamic Conditional Correlation Multivariate GARCH*. Working Paper 8554. NBER. DOI: 10.3386/w8554.

Haugh, Martin (2016). *A Brief Introduction to Stochastic Calculus*. Tech. rep. Columbia University, IEOR E4706: Foundations of Financial Engineering. URL: https://www.columbia.edu/~mh2078/FoundationsFE/IntroStochCalc.pdf.

Heston, Steven L. (1993). "A Closed-Form Solution for Options with Stochastic Volatility with Applications to Bond and Currency Options". In: *The Review of Financial Studies* 6.2, pp. 327–343. DOI: 10.1093/rfs/6.2.327.

Kolari, James W., Wei Liu, and Seppo Pynnönen (2024). "Portfolio Performance Measures". In: *Professional Investment Portfolio Management: Boosting Performance with Machine-Made Portfolios and Stock Market Evidence*. Cham: Springer Nature Switzerland, pp. 97–119.

Lindström, Erik, Henrik Madsen, and Jan Nygaard Nielsen (2018). *Statistics for Finance*. Chapman and Hall/CRC.

MathWorks, Inc. (2025). *lsqnonlin - Solve nonlinear least-squares (nonlinear data-fitting) problems*. Documentation, Optimization Toolbox. MathWorks. URL: https://se.mathworks.com/help/optim/ug/lsqnonlin.html.

Song, Xiaojun (2009). "Multivariate GARCH Models for the Greater China Stock Markets". Master's thesis. Singapore: Singapore Management University. URL: https://ink.library.smu.edu.sg/etd_coll/30.

Wiktorsson, Magnus (2025a). "Financial Statistics: Lecture 1 – Introduction and Stylized Facts". Lecture notes, course FMSN60/MASM18 Financial Statistics.

— (2025b). *Lecture 5: Conditional Variance Models*. Lecture notes, FMSN60/MASM18 Financial Statistics. Unpublished lecture notes.

— (2025c). *Lecture 6: Advanced Variance Models*. Lecture notes, FMSN60/MASM18 Financial Statistics. Lecture notes, Lund University.

Yahoo Finance (2026). *Coffee Futures (KC=F) Historical Prices*. Online. Accessed: 2026-01-07. URL: https://finance.yahoo.com/quote/KC%3DF/history/?guce_referrer=aHR0cHM6Ly93d3cuZ29vZ2xlLmNvb
guce_referrer_sig=AQAAAGTfMMpYSiCL4pWcYEkcm5wAtSLD9mCjtv0UIni7QSb0T5kzU2eiifdooS5ETdno4C2L_
WY7AotoSs-ctKhlSrQe4XyNtmz7IM-9lt0-wR1lIcROoh1b2L-rBMPbTMyMirPS7g78O-CsRWfdm62LgRwlKW0dz67XpV7C
period1=1478476800&period2=1481068800&guccounter=2.

Zaevski, Tsvetelin S., Young Shin Kim, and Frank J. Fabozzi (2014). "Option pricing under stochastic volatility and tempered stable Lévy jumps". In: *International Review of Financial Analysis* 31, pp. 101–108. ISSN: 1057-5219. DOI: 10.1016/j.irfa.2013.10.004. URL: https://www.sciencedirect.com/science/article/pii/S1057521913001403.